Photochemical & Photobiological Sciences

PERSPECTIVE

Cite this: *Photochem. Photobiol. Sci.*, 2018, **17**, 1691

Recent strategies to improve boron dipyrromethene (BODIPY) for photodynamic cancer therapy: an updated review

Chin Siang Kue,†[a] Shie Yin Ng,†[b] Siew Hui Voon,[c] Anyanee Kamkaew,[d] Lip Yong Chung,*[b] Lik Voon Kiew[e] and Hong Boon Lee*[b]

Received 18th March 2018,
Accepted 11th May 2018

DOI: 10.1039/c8pp00113h

rsc.li/pps

BODIPYs are photosensitizers activatable by light to generate highly reactive singlet oxygen ($^1O_2$) from molecular oxygen, leading to tissue damage in the photoirradiated region. Despite their extraordinary photophysical characteristics, they are not featured in clinical photodynamic therapy. This review discusses the recent advances in the design and/or modifications of BODIPYs since 2013, to improve their potential in photodynamic cancer therapy and related areas.

1. Introduction

Photosensitizers refer to a group of drugs that is only activated in the presence of light to generate reactive oxygen species from oxygen molecules. The $^1O_2$ generated is highly reactive towards biomolecules causing stress and necrosis to biological tissues. To date, many photosensitizers, such as chlorin e6, photofrin (porfimer sodium) and verteporfin, have undergone clinical trials for photodynamic cancer therapy (Clinicaltrial.gov: NCT03346304, NCT02916745, NCT00436553). Boron dipyrromethene (BODIPY), a non-tetrapyrrolic photosensitizer was found to possess favourable extinction coefficients, light to dark toxicity ratio, and thus is widely investigated as a potential photosensitizer in PDT and a fluorescent probe in molecular imaging. However, the core BODIPY structure generally possesses limitations such as high hydrophobicity, which limits the route of administration. Additionally, its low quantum fluorescence leads to dim fluorescence, low photostability results in low $^1O_2$ generation, and its short light absorption wavelength restricts its use only for the treatment of surface lesions, as the short wavelength light required for the BODIPY activation often fails to penetrate deep into the body. These limitations can be overcome by further modifying the structures. For instance, by making hydrophobic BODIPY more hydrophilic while maintaining a hydrophobic pouch for drug–cell interaction. This will produce higher singlet–triplet intersystem crossing for $^1O_2$ species generation, and near-infrared activatable BODIPY for deep tissue penetration. A comprehensive review on BODIPY in PDT was carried out by our group in 2013.[1] In this review, we update on new structural derivatives of BODIPY (Part A), as well as new strategies to enhance the delivery or efficacy of BODIPY (Part B). Only new BODIPYs reported after 2012 with demonstrated utility in photodynamic anticancer therapy and at least with proof of concept in *in vitro* settings have been included.

2. Part A: Modification on BODIPY structures

Photosensitizers need to be light-activated in order to generate reactive oxygen species (ROS) to perform PDT. Upon light irradiation, some photosensitizers undergo intersystem crossing (ISC) and rapidly form triplet excited states (T_1). T_1 can either transfer electron/proton directly to cellular organic substrates (lipids, proteins, nucleic acids, *etc.*), yielding free radicals that interact with O_2 to produce ROS such as hydrogen peroxide, the superoxide anion and the hydroxyl radical (Type-I reaction) or transfer its energy to the ground state O_2 to form highly reactive $^1O_2$ (Type-II reaction). $^1O_2$ produced through the Type-II reaction is thought to be mainly responsible for the cell death induced by PDT. The majority of photosensitizer development work has therefore focused on enhancing ISC, stabilizing T_1 and generation of $^1O_2$. Approaches attempted so

[a]*Department of Diagnostic and Allied Health Sciences, Faculty of Health and Life Sciences, Management & Science University, 40100 Shah Alam, Selangor, Malaysia. E-mail: hongboonlee@um.edu.my, hongboonlee@gmail.com*
[b]*Department of Pharmacy, Faculty of Medicine, University of Malaya, 50603 Kuala Lumpur, Malaysia. E-mail: chungly@um.edu.my, chungly@hotmail.com*
[c]*Project Leadership, Clinical Operations, R&D Solutions, IQVIA, 50480 Kuala Lumpur, Malaysia*
[d]*School of Chemistry, Institute of Science, Suranaree University of Technology, Nakhon Ratchasima 30000, Thailand*
[e]*Department of Pharmacology, Faculty of Medicine, University of Malaya, 50603 Kuala Lumpur, Malaysia*
†These authors contributed equally to this manuscript.

far include modification on BODIPY structures, *via* inclusion of heavy atoms, attachment of electron-withdrawing or electron-donating groups, designing of orthogonal dimers and introduction of transition-metal complexes.

I. Halogenated BODIPYs

While a photosensitizer's ability to generate $^1O_2$ from T_1 is key to the success of PDT, BODIPY photosensitizers, however, usually suffer from low singlet oxygen quantum yields ($^1O_2$ QYs). This is because the absorbed light energy typically stays at singlet excited states (S_n) rather than undergo ISC and is released as fluorescence.[2] In an effort to develop efficient PDT agents, incorporation of heavy atoms has been considered as an effective approach to enhance spin–orbital coupling (SOC) and thus facilitate singlet-to-triplet ISC and improve $^1O_2$ QYs of BODIPYs.[3,4] Belfield and co-workers designed a new halogenated BODIPY derivative **1**, by incorporating two iodine substituents at the 2- and 6-positions as heavy atoms, as well as a polyethylene glycol chain to improve water solubility. BODIPY **1** exhibited a high $^1O_2$ QY of 0.93 and, unsurprisingly, a low fluorescence quantum efficacy of 0.02. This heavy atom effect translated to observed photocytotoxicity on LLC Lewis lung carcinoma cells, with an IC_{50} of 10 μM.[3]

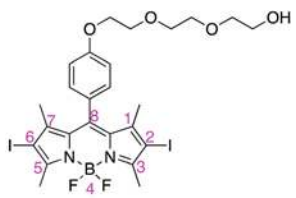

1

Acetonitrile
$\lambda_{max\ abs}$ = 528 nm
$\lambda_{max\ emiss}$ = 546 nm
ε = 75 500 M^{-1} cm^{-1}
Φ_f (Acridine) = 0.02 ± 0.002
$^1O_2$ QY (Acridine) = 0.93 ± 0.09
IC_{50} (LLC cells) = 10 μM (2.1 J cm^{-2})

As iodine is a "heavier" atom than bromine, attaching an iodine to BODIPY can usually result in a more drastic heavy atom effect than attaching a bromine.[1] However, incorporation of heavy atoms is not the only factor affecting $^1O_2$ QY, structural configuration will also affect $^1O_2$ QY of BODIPYs. To this end, Dong and co-workers synthesized a series of halogenated (brominated or iodinated) BODIPY derivatives, with either one or two BODIPY units joined together *via* a benzene ring.[4] Diiodinated **2a** exhibited the highest $^1O_2$ QY of 73%, which was higher than that of the corresponding di-brominated BODIPY (31%, structure not shown). Dimeric **2b** with four I atoms had a marginally lower $^1O_2$ QY of 68% compared to **2a** (two I atoms), probably due to the interplay between the heavy atom effect and the dimeric configuration of BODIPY. As expected, MTT assay revealed that **2a** had the lowest IC_{50} of only 0.6 μg mL^{-1} on HeLa cells and an *in vivo* study demonstrated that **2a** efficiently inhibited tumor growth in nude mice. It is worth noting that in the case of **2b**, conjugating more heavy atoms to the dimeric BODIPY also resulted in some dark cytotoxicity, where the cell viability dropped to 50% at a concentration of 100 μg mL^{-1}.

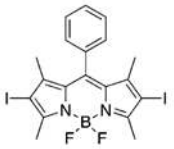

2a

Dichloromethane
$\lambda_{max\ abs}$ = 533 nm
$^1O_2$ QY (Methylene blue) = 0.73
IC_{50} (HeLa cells) = 1 μM (19.2 J cm^{-2})

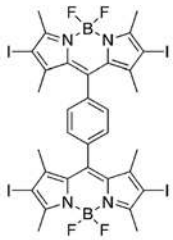

2b

Dichloromethane
$\lambda_{max\ abs}$ = 540 nm
$^1O_2$ QY (Methylene blue) = 0.68
IC_{50} (HeLa cells) = 2.8 μM (19.2 J cm^{-2})

Most research studies have focused on improving the $^1O_2$ generation efficiency of BODIPYs, but equally important is the bioavailability of $^1O_2$ at the target tissue for effective PDT. $^1O_2$ is a highly reactive species with a short half-life in biological systems (half-life ~ 2.0 μs); so, delivering of PDT agents as close as possible to their biotarget is important. Wang and coworkers synthesized two new NIR-absorbing halogenated distyryl BODIPYs (brominated **3a** and iodinated **3b**) to target and photocleave DNA.[5] The fluorescence quantum yields of **3a** and **3b** were low while their $^1O_2$ QYs were moderate (0.1 and 0.22 for **3a** and **3b** respectively) showing the stronger heavy-atom effect of iodine compared to bromine. The presence of the pyridinium group brought about amphiphilic characteristics to **3a** and **3b** ($\log P$ = 0.29 and 0.34, respectively). The binding affinity of **3a** and **3b** towards circulating tumor (CT) DNA was studied by absorption titration, circular dichroism spectroscopy, viscosity experiments and EB displacement assays. All the studies showed intercalation of BODIPYs **3a** and **3b** with CT DNA. Subsequent DNA photocleavage experiments indicated higher photocleavage activity for **3b** compared to **3a**, in accordance with its higher DNA affinity and $^1O_2$ QY. Interestingly, iodinated **3b** was shown to photocleave DNA exclusively through $^1O_2$, while brominated **3a** through both $^1O_2$ and hydroxyl radical ($^{\bullet}OH$). The authors claimed that this was the first detailed study showing the ability of BODIPYs to generate both $^1O_2$ and $^{\bullet}OH$ species, and may create a new opportunity to develop more efficient PDT agents.

A highly photostable bromo-substituted BODIPY dye (**4**) fused-ring-expanded with two thienopyrrole moieties was synthesized by Shen and co-workers.[6] Thiophene substituents were selected because of their lower electron delocalization energy barrier and more efficient π-conjugation capability relative to benzene – features important for enhancing ISC.[7] Three bromine atoms were also incorporated to further facilitate efficient ISC. The resulting structure showed red-shifted NIR λ_{max} at 698 nm. *In vitro* photocytotoxicity MTT assay using HeLa cells revealed that **4** exhibited high photocytotoxicity (IC_{50} = 7.12 μM) and no dark toxicity. Confocal fluorescence

imaging and flow cytometric analyses using Annexin V-FITC to study apoptosis further corroborated the MTT results.

3a
Acetonitrile
$\lambda_{max\ abs}$ = 648 nm
$\lambda_{max\ emiss}$ = 680 nm
ε = 45 000 M^{-1} cm^{-1}
Φ_f (Methylene Blue) = 0.095
$^1O_2$ QY (Methylene Blue) = 0.10

3b
Acetonitrile
$\lambda_{max\ abs}$ = 649 nm
$\lambda_{max\ emiss}$ = 686 nm
ε = 56 000 M^{-1} cm^{-1}
Φ_f (Methylene Blue) = 0.014
$^1O_2$ QY (Methylene Blue) = 0.22

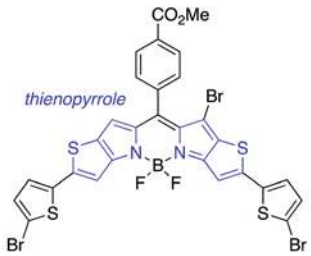

4
Dichloromethane
$\lambda_{max\ abs}$ = 698 nm
$\lambda_{max\ emiss}$ = 724 nm
ε = 230 000 M^{-1} cm^{-1}
Φ_f (Thienopyrrole-expanded BODIPY **4** without Bromine) = 0.04
$^1O_2$ QY (Methylene blue) = 0.63
IC_{50} (HeLa cells) = 7.12 μM

Cosa and co-workers prepared two halogenated BODIPYs, brominated **5a** and iodinated **5b**, featuring an electron-withdrawing acetoxymethyl group at the *meso*-position[8] to study their resistance against $^1O_2$ mediated photodegradation. **5a** and **5b** showed improved photostability against $^1O_2$ (relative efficiencies, E_{rel} = 91 for brominated **5a** and E_{rel} = 33 for iodinated **5b**) compared to a BODIPY with no acetoxymethyl group (E_{rel} = 20), without significantly affecting their $^1O_2$ QY (Φ_Δ = 0.84 for **5a** and Φ_Δ = 0.98 for **5b**, as compared to Rose Bengal, Φ_Δ = 0.54). The results revealed that bromine atoms conferred more stability to the photosensitizer than iodine atoms, probably because the former are more electron-withdrawing. Another reason may be due to the production of less oxidants by **5a** compared to **5b** as evident by their $^1O_2$ QYs. In *in vitro* assays using HeLa cervical cancer cells, **5a** and **5b** were shown to efficiently induce light-dependent apoptosis at EC_{50} = 140 nM and 180 nM, respectively. The better photocytotoxicity of **5a** compared to **5b** may be a direct result of the higher photostability of the brominated photosensitizer.

5a
Acetonitrile
$\lambda_{max\ abs}$ = 543 nm
Φ_f = 0.14
$^1O_2$ QY (Rose Bengal) = 0.84
EC_{50} (HeLa cells) = 140 nM (4.68 J cm^{-2})

5b
Acetonitrile
$\lambda_{max\ abs}$ = 550 nm
Φ_f = N.D
$^1O_2$ QY (Rose Bengal) = 0.98
EC_{50} (HeLa cells) = 180 nM (4.68 J cm^{-2})

II. Non-halogenated BODIPYs

Two-photon-absorption PDT (TPA-PDT) has attracted great interest recently due to its in-depth tissue penetration.[9] TPA is a process by which a molecule can simultaneously absorb a pair of photons in the presence of intense laser pulses, the sum of whose energy equals the transition energy to singlet excited states. The relatively longer laser wavelength employed results in a deeper penetration of light into tissue.[10] Xing and co-workers synthesized a new amphiphilic BODIPY-porphyrin conjugate **6a** capable of performing TPA-PDT, together with its precursor **6b**.[11] Conjugate **6a** consists of a hydrophobic BODIPY connected with zinc porphyrin *via* an acetylide linker at its *meso* position. The hydrophilicity of **6a** is contributed by two tri(ethylene glycol) chains and a tetra(ethylene glycol) chain bridging a cationic triphenylphosphonium group, separately conjugated to the remaining three *meso* positions of the zinc porphyrin core. Both compounds exhibited a low fluorescence intensity (Φ_f = 0.015 for **6a** and 0.016 for **6b**). Using *meso*-tetraphenylporphyrin (H_2TPP) as reference (Φ_Δ = 0.55 in $CHCl_3$), the relative $^1O_2$ QYs of BODIPY **6a** and **6b** were determined to be 0.52 and 0.59, respectively. TPA cross-sections (TPCS) were investigated using the *Z*-scan method: **6a** exhibited a large TPCS of 1725 GM, whereas **6b** had 1673 GM, comparing with the reference compound (conjugate **6b** without BODIPY), which had a lower TPCS of 1154 GM. Large TPCS can be utilized to enhance two-photon excitation fluorescence emission, as well as two-photon excitation $^1O_2$ generation. *In vitro* cellular uptake studies showed that **6a** demonstrated rapid and efficient cellular uptake in human breast carcinoma MCF-7 cells, which was about 80% higher than that of **6b**. This can be attributed to the more favorable log *P* value of **6a** than **6b** (1.09 *vs.* 5.15) for facilitating transport across the cell membrane. *In vitro* photocytotoxicity studies using 0.5–1.5 J cm^{-2} with a 500 nm long-pass filter showed that **6a** exhibited greater photocytotoxicity than **6b**, in accordance with the superior cellular uptake data. This photocytotoxicity trend was also observed in experiments conducted using two-photon laser irradiation from 0–9.6 J cm^{-2} at 900 nm (one laser shot per min).

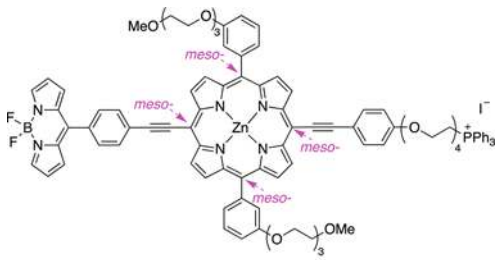

6a

DMSO
$\lambda_{max\ abs}$ = 449 nm, 505 nm, 659 nm
$\lambda_{max\ emiss}$ = 665 nm
Φ_f (Zinc tetraphenylporphyrin) = 0.015
$^1O_2$ QY (H_2TPP) = 0.52
Cytotoxicity (MCF-7 cells) = 30 – 80 % (0.5 – 1.5 J cm^{-2})

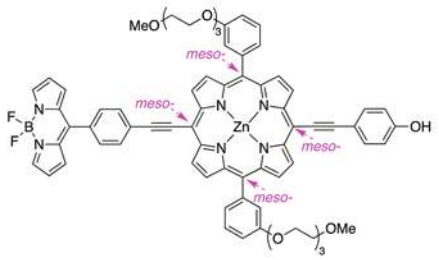

6b

DMSO
$\lambda_{max\ abs}$ = 450 nm, 505 nm, 660 nm
$\lambda_{max\ emiss}$ = 666 nm
Φ_f (Zinc tetraphenylporphyrin) = 0.016
$^1O_2$ QY (H_2TPP) = 0.59
Cytotoxicity (MCF-7 cells) = 20 – 40 % (0.5 – 1.5 J cm^{-2})

As widely acknowledged, designing a photosensitizer with high fluorescence and high photocytotoxic ability is challenging as fluorescence emission and $^1O_2$ generation are competing decay processes of the excited states of a photosensitizer. You and co-workers reported a rare phenomenon where a thieno-pyrrole fused BODIPY was able to generate more $^1O_2$ without having any heavy halogen atoms, while maintaining a moderate fluorescence quantum yield – a characteristic that is desirable for effective dual theranostic clinical applications.[12] In the study, the authors examined the electronic effects of thieno-pyrrole fused BODIPYs with respect to $^1O_2$ generation, by attaching hydrogen (**7a**), electron-withdrawing CF_3 (**7b**) or electron-donating CH_3 (**7c**) groups at the *para*-position of a thieno-pyrrole BODIPY. While electron-donating **7c** did not show any detectable $^1O_2$ QY, neutral **7a** and electron-accepting **7b** showed moderate $^1O_2$ QY (~0.4). All three analogues maintained moderate Φ_f (0.2–0.6). It was discovered that $^1O_2$ QY correlated with the HOMO–LUMO energy gap, which was the largest for **7b**. Even though **7b** had slightly better singlet oxygen generation and fluorescence properties than **7a**, the latter was selected for *in vitro* and *in vivo* assay because **7b** was insoluble in aqueous solution. **7a** had no dark toxicity up to 5.0 μM and showed photocytotoxicity (IC_{50} = 3.0 μM) when irradiated with 10 J cm^{-2} of light. *In vivo* antitumor experiments of **7a** (5 μM kg^{-1}, 150 J cm^{-2} of light) showed dramatic reduction in tumors on Balb/c tumor-bearing mice, from 100 mm^3 at day 0 to nearly 0 mm^3 at day 1, with no palpable tumors up to 60 days post-treatment. *In vivo* imaging was conducted and bright fluorescence signals were observed in tumor and skins, and the emission intensity from the skin decreased more quickly than that from the tumor suggesting a degree of selective retention in tumor. In *ex vivo* imaging, the lung, liver and heart showed a relatively high emission intensity compared to other excised organs.

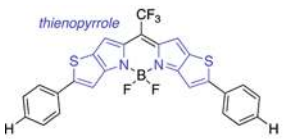

7a

Chloroform
$\lambda_{max\ abs}$ = 688 nm
$\lambda_{max\ emiss}$ = 700 nm
ε = 120 000 M^{-1} cm^{-1}
Φ_f (Aza BODIPY) = 0.22
$^1O_2$ QY [Ru(bipy)$_3$]Cl$_2$ = 0.42
IC_{50} (colon-26 cells) = 3 μM (10 J cm^{-2})

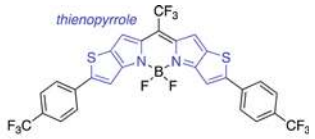

7b

Chloroform
$\lambda_{max\ abs}$ = 688 nm
$\lambda_{max\ emiss}$ = 695 nm
ε = 211 000 M^{-1} cm^{-1}
Φ_f (Aza BODIPY) = 0.39
$^1O_2$ QY [Ru(bipy)$_3$]Cl$_2$ = 0.47
IC_{50} (colon-26 cells) = N.D

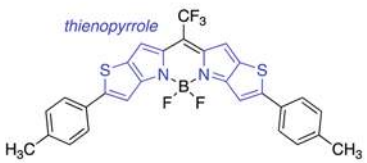

7c

Chloroform
$\lambda_{max\ abs}$ = 709 nm
$\lambda_{max\ emiss}$ = 712 nm
ε = 287 000 M^{-1} cm^{-1}
Φ_f (Aza BODIPY) = 0.67
$^1O_2$ QY [Ru(bipy)$_3$]Cl$_2$ = N.D
IC_{50} (colon-26 cells) = N.D

Besides halogenation, development of efficient BODIPYs for PDT can also be achieved through a non-halogenate approach. One way is to attach a functional group that donates electrons to stabilize the photoexcited BODIPY core and to quench fluorescence, thereby promoting a triplet-state lifetime.[13] Based on this strategy, Chang and co-workers attached electron-donating aniline units to generate 3,5-dianiline-substituted (**8a**) and 2,6-dianiline-substituted BODIPY (**8b**).[14] **8a** and **8b** showed comparable $^1O_2$ QYs (0.40 and 0.38 respectively) when measured against methylene blue (MB) (Φ_Δ = 0.52 in D_2O). Different to **8b** and MB, **8a** showed high photostability under irradiation conditions (6 mW cm^{-2} at 400–700 nm) and was selected for further testing. Irradiation-time-dependent fluorescent images of **8a** showed photodamage to cancer cells but not to normal cells, indicating its selective PDT properties. This corroborated with the subcellular localization experiments of **8a** that showed major localization in the endoplasmic reticulum (ER) and weak fluorescence in the mitochondria of HeLa cancer cells, but no apparent colocalization between **8a** and the trackers in normal cells. MTT assay on three cancer cell lines exhibited phototoxicity (EC_{50} values of 4.7, 6.8, and 18.5 μM for HeLa, A549 and MRC-5, respectively) and no observable dark toxicity up to 15 μM. To find out whether **8a** also produced hydroxyl radicals and/or superoxide anion (*via* Type-I reaction), the free-radical probe 4-((9-acridinecarbonyl)amino)-2,2,6,6-tetramethylpiperidin-1-oxyl (TEMPO-9-ac) was used. As irradiation of **8a** at 6 mW cm^{-2} generated a more apparent increase in emission signal from TEMPO-9-ac compared to the

unchanged level of the control (TEMPO-9-ac), **8a** concluded to undergo both Type-I and -II PDT reactions.

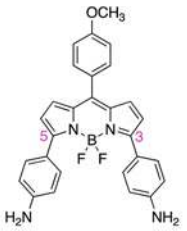

8a

Toluene
Φ_f (Rhodamine B) = 0.16
$^1O_2$ QY (Methylene Blue) = 0.40
EC_{50} (HeLa cells) = 4.7 μM (8 J cm^{-2})
EC_{50} (A549 cells) = 6.8 μM (8 J cm^{-2})
EC_{50} (MRC-5 cells) = 18.5 μM (8 J cm^{-2})

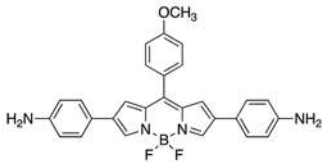

8b

Toluene
Φ_f (Rhodamine B) = 0.16
$^1O_2$ QY (Methylene Blue) = 0.38
EC_{50} (HeLa cells) ~ 5.8 μM (8 J cm^{-2})
EC_{50} (A549 cells) ~ 6.7 μM (8 J cm^{-2})
EC_{50} (MRC-5 cells) ~ 6.9 μM (8 J cm^{-2})

Another way to change the $^1O_2$ generation ability of photosensitizers without any heavy atoms is to prepare orthogonal BODIPY dimers. In spite of efforts in the field, the ability to generate abundant singlet oxygen in orthogonal BODIPY dimers is still not well understood. Even less well understood is how solvent polarity or substitution pattern affects the SOG ability of orthogonal BODIPY dimers. For this reason, Ortiz and co-workers prepared a new library of orthogonal BODIPY dimers with different substitution patterns and studied their behaviour in solvents of different polarity.[15] BODIPY dimer **9a** featuring two identical BODIPY units covalently linked together at their corresponding 2- and 8′-BODIPY positions was the basic reference structure for the other derivatives. First, the effect of solvent polarity on **9a** was studied using cyclohexane (non-polar), $CHCl_3$ (intermediate polarity) and CH_3CN (very high polarity). The highest $^1O_2$ QY was recorded in the medium polar $CHCl_3$. Next, it was noted that introducing an electron donating $-NH_2$ resulted in **9b** with higher $^1O_2$ QY (0.85) than **9a** when compared in chloroform (0.75). Conversely, the presence of a nitrophenyl group with electron-withdrawing character (**9c**) led to reduction in $^1O_2$ generation (Φ_Δ = 0.43). Introduction of thienyl at the 2-, 6- and 6′-positions of both BODIPY units (structures not shown) was carried out to study the effect of asymmetric extension of π-conjugation on the photophysical properties. Overall, the spectral bands in these asymmetric dimers were shifted to the red. More interestingly, the asymmetric dimers showed both moderate fluorescence and singlet oxygen production with relatively high extinction coefficients up to 600 nm, offering the opportunity to explore dual functionality for theranostic clinical applications for these dimers. The *in vitro* activity of selected dimers was investigated on HeLa cells, where they were shown to internalize into cells, exhibit low dark and high photocytotoxicity even at nanomolar concentrations (50 nM for **9a**). The photocytotoxicity profile of the dimers generally correlate with the dimers' photophysical parameters such as the absorption coefficient and singlet oxygen quantum yield.

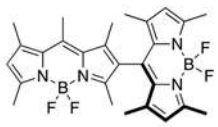

9a

Chloroform
$\lambda_{max\ abs}$ = 505 nm
$\lambda_{max\ emiss}$ = 527 nm
ε = 180 000 M^{-1} cm^{-1}
Φ_f = 0.22
$^1O_2$ QY (8-Methylthio-2,6-diiodo-BODIPY) = 0.75

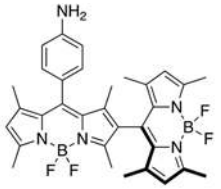

9b

Chloroform
$\lambda_{max\ abs}$ = 510 nm
$\lambda_{max\ emiss}$ = 526 nm
ε = 81 000 M^{-1} cm^{-1}
Φ_f = 0.05
$^1O_2$ QY (8-Methylthio-2,6-diiodo-BODIPY) = 0.85
Surviving fraction (HeLa cells) = 5% at 0.25 μM (5 J cm^{-2})

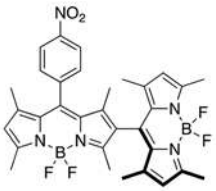

9c

Chloroform
$\lambda_{max\ abs}$ = 513 nm
$\lambda_{max\ emiss}$ = 532/675 nm
ε = 151 000 M^{-1} cm^{-1}
Φ_f = < 0.01
$^1O_2$ QY (8-Methylthio-2,6-diiodo-BODIPY) = 0.43

III. BODIPY-metal complexes

Introducing transition-metal ions in close proximity to a fluorophore skeleton is another approach to enable the observation of excited triplet states. In that context, a range of transition-metal complexes of BODIPY-based fluorophores have been designed and investigated as triplet photosensitizers. Although conceptually inspiring, transition-metal complexes showing fluorescence emission together with effective intersystem crossing (ISC) are still at an early stage of development; the major challenge probably being the simultaneous activation of these two photophysically opposed processes under visible light.[16]

Cyclometalated Ir^{III} complexes have recently received great interest for PDT agents due to their exceptional properties such as simple color tuning, energy-level control, high quantum yields, large Stokes shifts, long-lived phosphorescence, and ROS generation under hypoxia conditions *via* electron (type I) or energy transfer (type II).[17] Zhao and co-workers prepared four heteroleptic cyclometalated Ir(III) complexes (**10a–d**) using BODIPY ligands.[18] A π-conjugation linker (–C≡C– triple bond) was used to maximize the heavy atom effect exerted by Ir(III) on the styryl BODIPY ligand, to access absorption/fluorescence in the NIR region as well as long-lived triplet excited states and efficient ISC. **10b** has a high molar

absorption coefficient at 664 nm, moderate fluorescence in the NIR region, and high $^1O_2$ QY (Φ_Δ = 0.81), exhibits predominate photocytotoxicity over dark cytotoxicity in LLC cells (lung cancer cells) upon irradiation, making it potentially suitable for use in *in vivo* photodynamic therapy (PDT).

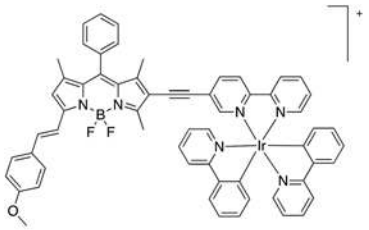

10a
toluene
$\lambda_{max\ abs}$ = 606 nm
$\lambda_{max\ emiss}$ = 624 nm
ε = 114000 M^{-1} cm^{-1}
Φ_f = 0.399
$^1O_2$ QY (methylene blue) = 0.53
IC_{50} (1211 cells) = 2.58 μM
IC_{50} (LLC cells) = 6.18 μM

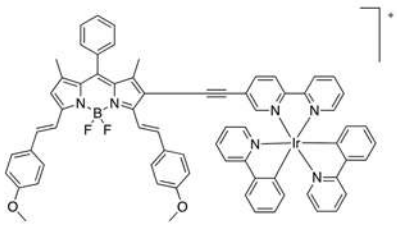

10b
toluene
$\lambda_{max\ abs}$ = 664 nm
$\lambda_{max\ emiss}$ = 691 nm
ε = 89600 M^{-1} cm^{-1}
Φ_f = 0.132
$^1O_2$ QY (methylene blue) = 0.81
IC_{50} (1211 cells) = 7.68 μM
IC_{50} (LLC cells) = 9.80 μM

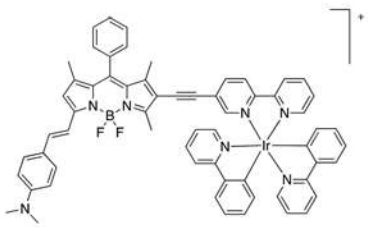

10c
toluene
$\lambda_{max\ abs}$ = 644 nm
$\lambda_{max\ emiss}$ = 683 nm
ε = 98900 M^{-1} cm^{-1}
Φ_f = 0.326
$^1O_2$ QY (methylene blue) = 0.06

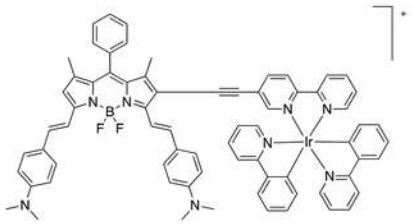

10d
toluene
$\lambda_{max\ abs}$ = 729 nm
$\lambda_{max\ emiss}$ = 794 nm
ε = 78900 M^{-1} cm^{-1}
Φ_f = 1.000
$^1O_2$ QY (methylene blue) = 0.02

Ortiz and co-workers successfully designed and synthesized dual fluorescent-PDT materials based on acetylacetonated BODIPY chelating biscyclometalated Ir^{III} (**11a** and **11b**).[19] The direct incorporation of stabilized 1,3-diketonate nucleophilic groups, with well-known chelating properties, to the *meso* position of BODIPYs renders the complexes with good photophysical properties (high absorption coefficients, moderate fluorescence emission and efficient $^1O_2$ generation upon visible-light irradiation), while leaving the 2- and 6-BODIPY positions available for further functionalization to finely modulate the photophysical properties of the final material (*i.e.*, shifting the absorption to the red by incorporating π-systems). A comprehensive computationally aided (DFT) photophysical study, based on conventional steady-state and time-resolved UV/Vis spectroscopy, demonstrates that **11a** and **11b** exhibit an ideal balance between fluorescence emission and $^1O_2$ generation, making them suitable as efficient organometallic fluorescent-PDT agents. *In vitro* photodynamic therapy (PDT) activity studied for **11a** and **b** in HeLa cells shows that such complexes are efficiently internalized into the cells, exhibiting low dark- and high photocytoxicity, even at significantly low complex concentrations, making them potentially suitable as theranostic agents.

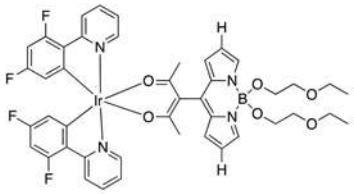

11a
acetonitrile
$\lambda_{max\ abs}$ = 517 nm
$\lambda_{max\ emiss}$ = 628 nm
ε = 446000 M^{-1} cm^{-1}
Φ_f = 0.08
$^1O_2$ QY (Rose Bengal) = 0.86
IC_{50} (HeLa cells) = 50 nM (6.8 J cm^{-2})

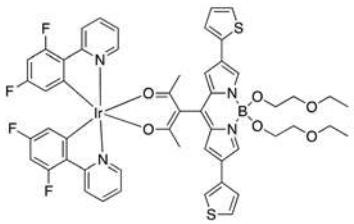

11b
acetonitrile
$\lambda_{max\ abs}$ = 597 nm
ε = 33800 M^{-1} cm^{-1}
Φ_f = 0.22
$^1O_2$ QY (methylene blue) = 0.60
IC_{50} (HeLa cells) = 1-5 μM (6.8 J cm^{-2})

A new class of cyclometalated iridium(III) with NCN pincer and *meso*-phenylcyanamide BODIPY ligands (**12a** & **12b**) have been synthesized by Tabrizi and Chiniforoshan and studied for combined PDT and chemotherapy.[20] The DNA-binding interactions of the complexes with calf thymus DNA display that the binding mode is mainly non-covalent *via* intercalation. The complexes showed cleavage of SC-DNA efficiently on photoactivation at 500 nm with the formation of reactive $^1O_2$ as the main contributor. The complexes showed good uptake, efficient ROS generation and are less toxic in the dark (IC_{50} ~ 60 μM) than upon light irradiation (500 nm) when tested in HeLa cells (IC_{50}values of 0.78 ± 0.1 mM and 0.53 ± 0.1 mM respectively). Moreover, the complexes revealed exceptional TrxR-inhibitory activities in comparison with auranofin, suggesting that the selenoenzyme TrxR may act as a protein target for these Ir(III) complexes.

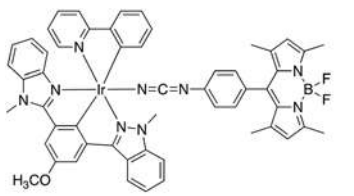

12a
acetonitrile
$\lambda_{max\ abs}$ = 541 nm
$\lambda_{max\ emiss}$ = 588 nm
$^1O_2$ QY = 0.71-0.79
IC_{50} (HeLa cells) = 0.78 μM (10 J cm^{-2})
IC_{50} (MRC-5 cells) = 24 μM (10 J cm^{-2})

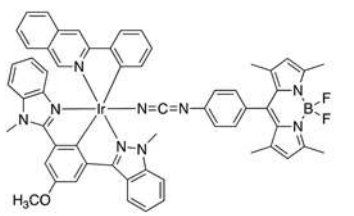

12b
acetonitrile
$\lambda_{max\ abs}$ = 526 nm
$\lambda_{max\ emiss}$ = 598 nm
$^1O_2$ QY = 0.88-0.92
IC_{50} (HeLa cells) = 0.53 μM (10 J cm^{-2})
IC_{50} (MRC-5 cells) = 31 μM (10 J cm^{-2})

Xie and coworkers designed and synthesized fluorescent cyclometalated Ir(III) complexes containing a BODIPY unit (IrBDP

or **13**), which could self-assemble into corresponding organic nanoparticles (IrBDP NPs).[21] The average hydrodynamic diameter determined by DLS was about 190.2 nm. Compared with IrBDP, the maximum absorption peak of IrBDP NPs bathochromic-shifted from 13 nm to 520 nm. The introduction of Ir(III) significantly increased the photodynamic effect of BDP due to the heavy atom effect but at the expense of decreased fluorescence quantum yield. The IrBDP NPs were taken up by cells, probably *via* endocytosis as localization in lysosomes was detected. In addition, phototoxicity against murine colon cancer (CT26) and human cervical carcinoma (HeLa) cell lines was validated.

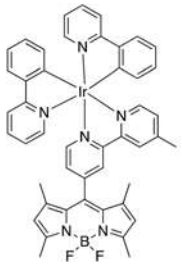

13

tetrahydrofuran
$\lambda_{max\ abs}$ = 507 nm
$\lambda_{max\ emiss}$ = 526 nm

IrBODIPY NPs

water
$\lambda_{max\ abs}$ = 520 nm
$\lambda_{max\ emiss}$ = 554 nm
IC_{50} (CT26 cells) = 0.04 μg mL^{-1} (28.8 J cm^{-2})
IC_{50} (HeLa cells) = 0.005 μg mL^{-1} (28.8 J cm^{-2})

Ruthenium complexes are drawing growing attention in the development of new anticancer drugs due to their rich and tunable chemical, photophysical and photochemical properties.[22] In PDT, many Ru complexes exhibit high $^1O_2$ quantum yields and therefore are attractive. In recent years, Ru complexes comprising photolabile ligand(s) have also been studied extensively as photoactivated chemotherapy (PACT) agents.[23] Wang *et al.* synthesized a BODIPY-modified pyridine ligand (py-BODIPY) and its iodinated counterpart (Py-I-BODIPY) and prepared 3 Ru arene complexes (**14a–c**) for PDT/PACT applications.[24] Efficient electron transfer from the singlet excited state of py-BODIPY to the Ru(II) arene moiety occurs in **14a**, which leads to fast dissociation of py-BODIPY from the Ru(II) center and allows for covalent binding of the resulting Ru residue to DNA. Due to the heavy atom effect from the iodine atoms, **14b** and **c** display high $^1O_2$ quantum yields and can cleave DNA effectively upon visible light irradiation, as well as photoinactivate human ovarian adenocarcinoma SKOV3 cells. The attractive photo-killing activities of **14b** and **c** are the result of the integration of both the iodized BODIPY and the Ru(II) arene moieties; the former provides potent $^1O_2$ activity and strong DNA intercalating ability, and the latter offers the complexes suitable water solubility and an additional electrostatic interaction with DNA.

Chakravarty and co-workers published a series of transition metal complexes appended with BODIPY (**15–19**) with a number of similar characteristics. The bodipy moiety was either 4,4-difluoro-1,3,5,7-tetramethyl-4-bora-3a,4a-diaza-*s*-indacene (complex **a**) or its 2,4-diiodo analogue (complex **b**) and conjugated to the metallic core at the *meso* position *via* a 4-methylphenyl group. The complexes showed strong absorption in the range of λ_{max} = 510–540 nm. The di-iodo complexes in these examples generated reactive oxygen species when induced by visible light, showed significant mitochondrial localization in cancer cells, and an excellent photodynamic therapy effect in visible light (400–700 nm) giving sub- to low micromolar IC_{50} values in cancer cells, while being less toxic in the dark. The authors' major interest in mitochondrial localization is to avoid the nuclear excision repair (NER) pathway, which reduces the efficacy of any nuclear DNA targeting anticancer drug by targeting instead the mitochondrial DNA.[25]

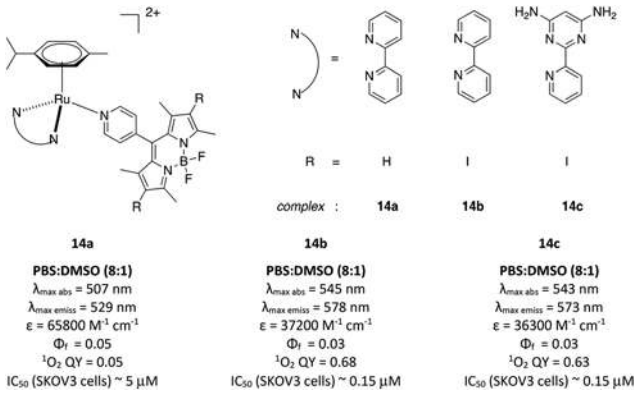

R = H I I
complex : **14a** **14b** **14c**

14a
PBS:DMSO (8:1)
$\lambda_{max\ abs}$ = 507 nm
$\lambda_{max\ emiss}$ = 529 nm
ε = 65800 M^{-1} cm^{-1}
Φ_f = 0.05
$^1O_2$ QY = 0.05
IC_{50} (SKOV3 cells) ~ 5 μM

14b
PBS:DMSO (8:1)
$\lambda_{max\ abs}$ = 545 nm
$\lambda_{max\ emiss}$ = 578 nm
ε = 37200 M^{-1} cm^{-1}
Φ_f = 0.03
$^1O_2$ QY = 0.68
IC_{50} (SKOV3 cells) ~ 0.15 μM

14c
PBS:DMSO (8:1)
$\lambda_{max\ abs}$ = 543 nm
$\lambda_{max\ emiss}$ = 573 nm
ε = 36300 M^{-1} cm^{-1}
Φ_f = 0.03
$^1O_2$ QY = 0.63
IC_{50} (SKOV3 cells) ~ 0.15 μM

In Cu(II) complexes **15a** and **b**,[26] the other complexing ligand, curcumin (1*E*,6*E*)-1,7-bis((4-hydroxy-3-methoxyphenyl) hepta-1,6-diene-3,5-dione), is known for its medicinal values, biocompatibility, potent anticancer activity and photosensitizing properties generating ROS and poor *in vivo* bioavailability due to rapid degradation of the curcumin dye in cellular medium limits. The authors were able to show that binding to copper(II) has rendered stability to curcumin from its hydrolytic degradation in buffer medium.

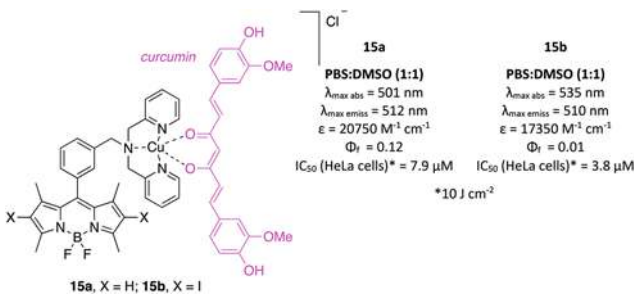

15a
PBS:DMSO (1:1)
$\lambda_{max\ abs}$ = 501 nm
$\lambda_{max\ emiss}$ = 512 nm
ε = 20750 M^{-1} cm^{-1}
Φ_f = 0.12
IC_{50} (HeLa cells)* = 7.9 μM

15b
PBS:DMSO (1:1)
$\lambda_{max\ abs}$ = 535 nm
$\lambda_{max\ emiss}$ = 510 nm
ε = 17350 M^{-1} cm^{-1}
Φ_f = 0.01
IC_{50} (HeLa cells)* = 3.8 μM

*10 J cm^{-2}

15a, X = H; **15b**, X = I

Another BODIPY-copper(II) complex **16**[27] has tumor cell targeting vitamin B_6 (VB_6) derived Schiff base as a ligand for targeted photo-chemotherapy that combines targeted chemotherapy with photodynamic therapy. The choice of vitamin B_6 (VB_6) as a tumor recognition moiety is based upon the fact that survival and proliferation of cancer cells require enhanced uptake of VB_6 to meet the elevated activity of enzyme serine hydroxymethyltransferase in DNA biosynthesis.

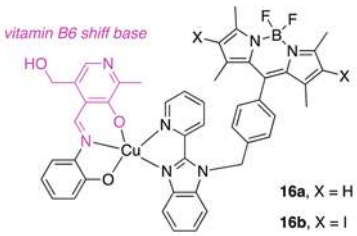

16a	16b
Dulbecco's PBS:DMSO (4:1)	**Dulbecco's PBS:DMSO (4:1)**
$\lambda_{max\ abs}$ = 500 nm	$\lambda_{max\ abs}$ = 535 nm
$\lambda_{max\ emiss}$ = 511 nm	-
ε = 17800 M^{-1} cm^{-1}	ε = 13700 M^{-1} cm^{-1}
Φ_f = 0.1	-
IC_{50} (HeLa cells)* = 12.4 μM	IC_{50} (HeLa cells)* = 0.60 μM
IC_{50} (MCF-7 cells)* = 6.05 μM	IC_{50} (MCF-7 cells)* = 0.43 μM
IC_{50} (HepG2 cells)* = 13.2 μM	IC_{50} (HepG2 cells)* = 0.64 μM

*10 J cm^{-2}

Another curcumin ligated metal complex by the same group is based on oxidovanadium(IV), **17**.[28] As before, the complexes are stable in a solution phase over a long period of time of 48 h without showing any apparent degradation of the curcumin ligand. Mechanistic data from pUC19 DNA photocleavage studies revealed photogenerated ROS as primarily $^1O_2$ from the BODIPY moiety and $^{\bullet}OH$ radicals from the curcumin ligand.

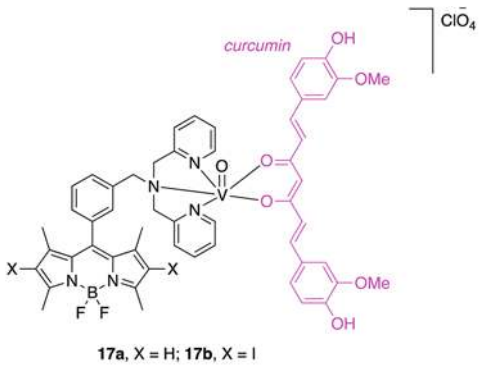

17a	17b
Dulbecco's PBS:DMF (1:1)	**Dulbecco's PBS:DMF (1:1)**
$\lambda_{max\ abs}$ = 501 nm	$\lambda_{max\ abs}$ = 535 nm
$\lambda_{max\ emiss}$ = 512 nm	$\lambda_{max\ emiss}$ = 521 nm
ε = 54680 M^{-1} cm^{-1}	ε = 30285 M^{-1} cm^{-1}
Φ_f = 0.11	Φ_f = 0.01
IC_{50} (HeLa cells)* = 5.8 μM	IC_{50} (HeLa cells)* = 2.5 μM
IC_{50} (MCF-7 cells)* = 6.2 μM	IC_{50} (MCF-7 cells)* = 2.7 μM

*10 J cm^{-2}

The same research group also reported two types of BODIPY-ligated Pt(II) complexes **18** and **19**. The BODIPY unit in each case was intended to direct the complexes to the mitochondria. For complex **18**,[29] where the bodipy unit is linked to 2-(2-pyridyl)benzimidazole before binding platinum in a bidentate mode, confocal microscopy images of **18a** and Pt estimation from isolated mitochondria showed colocalization of the complexes in the mitochondria while complex **18b** displayed generation of reactive oxygen species induced by visible light, disruption of the mitochondrial membrane potential, and apoptosis. For complex **19**,[30] the design is to effect mitochrondrial accumulation of the complex followed by slow release of the active platinum species to crosslink formation with the mt-DNA. The authors established accumulation in cellular mitochondria using confocal microscopy and formation of Pt-DNA adducts from binding experiments with 9-ethylguanine as a model nucleobase.

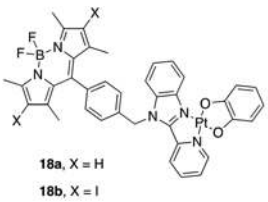

18a	18b
1% DMSO/Dulbecco's PBS	**1% DMSO/Dulbecco's PBS**
$\lambda_{max\ abs}$ = 510 nm	$\lambda_{max\ abs}$ = 550 nm
$\lambda_{max\ emiss}$ = 505 nm	-
ε = 16100 M^{-1} cm^{-1}	ε = 13700 M^{-1} cm^{-1}
Φ_f = 0.06	-
IC_{50} (HaCaT cells)* = 35.0 μM	IC_{50} (HaCaT)* = 2.9 μM

*10 J cm^{-2}

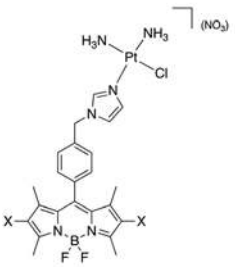

19a	19b
1% DMSO/Dulbecco's MEM	**1% DMSO/Dulbecco's MEM**
$\lambda_{max\ abs}$ = 530 nm	$\lambda_{max\ abs}$ = 540 nm
$\lambda_{max\ emiss}$ = 510 nm	-
ε = 18000 M^{-1} cm^{-1}	ε = 14000 M^{-1} cm^{-1}
Φ_f = 0.09	-
IC_{50} (HaCaT cells)* = 0.15 μM	IC_{50} (HaCaT)* = 0.10 μM
IC_{50} (MCF-7 cells)* = 6.7 μM	IC_{50} (MCF-7 cells)* = 2.6 μM

*10 J cm^{-2}

Other than Chakravarty and co-workers, Liu *et al.* reported a similar Pt-Bodipy **20** possessing near-IR absorption through introduction of 4-methoxystyrylbenzene substituents in the BODIPY to extend the π conjugation.[31] Similar to complex **19**, complex **20** was intended to effect simultaneous chemotherapy and PDT. While the ability to form DNA-Pt adducts was not tested, the researchers showed that complex **20** had comparable chemotherapeutic toxicity with cisplatin in the dark and superior PDT effects compared to precursor BODIPY, probably as a result of the heavy atom effect from Pt. *In vivo* NIR fluorescence imaging of tumor and inhibition of tumor xenograft in the dark were demonstrated.

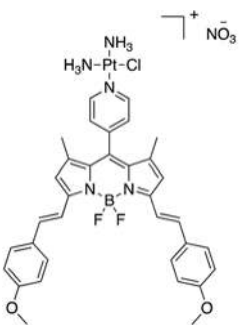

20

MeOH

$\lambda_{max\ abs}$ = 650 nm

$\lambda_{max\ emiss}$ = 682 nm

Φ_f (rhodamine 6G)= 0.08

IC_{50} (HepG2 cells) = 35 μM (38.4 J cm^{-2})

IC_{50} (HeLa cells) = 11 μM (38.4 J cm^{-2})

The first example of Au(I)-BODIPY complex **21** was reported by Ucuncu *et al.*[32] Upon complexation with Au(I), a photoinactive

BODIPY derivative was transformed into a highly photoactive triplet sensitizer. Along with high efficiency in $^1O_2$ generation (Φ_Δ = 0.84), the new BODIPY–Au(I) skeleton showed excellent photocytotoxic activity against cancer cell lines (EC_{50} = 2.5 nM).

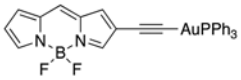

21

CH_2Cl_2
$\lambda_{max\ abs}$ = 550 nm
$\lambda_{max\ emiss}$ = 583 nm
ε = 38000 M^{-1} cm^{-1}
Φ_f (rhodamine B)= 0.05
$^1O_2$ QY = 0.84
EC_{50} (A549 cells) = 2.5 nM (38.4 J cm^{-1})

3. Part B: Strategies to enhance efficacy of BODIPY in photodynamic therapy

I. Targeting ligand

Active targeted therapy of cancer refers to targeting the surface molecules on cancer cells using a small molecule to deliver cargo for therapeutic or diagnostic purposes. The cargo can be a cytotoxic drug, an imaging probe or a photosensitizer.[33] Active targeted drug delivery reduces the toxicity of a drug by targeting the receptor of targeted cells but not the normal cells. For instance, Burgess and co-worker designed a peptidomimetic ligand targeting Tropomyosin receptor kinase C (TrkC) in cancer cells. In the design, conjugation of TrkC targeting ligands (IYIY) to diiodo-BODIPY gave structure **22a**.[34] Upon conjugation, the targeting properties was significantly increased compared to I_2-BODIPY (**22b**) as tested in both murine and human TrkC expressing cancer cell lines, where the IC_{50} = 0.325 μM in 4T1 (murine), IC_{50} = 0.285 μM in HS578t (human) cells compared to I_2-BODIPY, which had undetermined IC_{50} at a light dose of 7.3 J cm^{-2}. There was no cytotoxicity effect on the TrkC negative 67NR cell line under the same light dose and no dark toxicity. In animal studies, IYIY-I_2-BODIPY at 10 mg kg^{-1} was able to induce superior antitumor activity, with 96% tumor volume reduction in TrkC expressing 4T1 tumor at day 6 post-irradiation and among these mice, 71% was reported to show full remission with no tumor growth and metastasis up to 90 days of observation. Conversely, the I_2-BODIPY treated group at the equivalent dose showed 11% reduction in tumor volume at day 6 post-irradiation and regrowth at day 13.[35] Interestingly, the targeting IYIY ligand also possessed immunomodulation properties. Subjecting 4T1 tumor bearing mice to PDT, the same group demonstrated that IYIY-I_2-BODIPY was able to enhance the antitumor immune responses by increasing the IFN-γ^+ and IL-17^+ CD4 and CD8T cells, memory CD4 and CD8T cells, and reduced the immunosuppressive myeloid derived suppressive cells, regulatory T cells and immunosuppressive cytokines TGF-β. In contrast, I_2-BODIPY alone had a mild and insignificant increase in adaptive immunity compared to the untreated control group.[36]

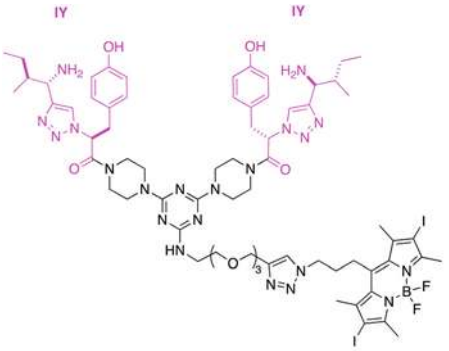

22a

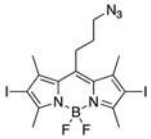

22b

DMSO
$\lambda_{max\ abs}$ = 532 nm
$\lambda_{max\ emiss}$ = 550 nm
ε = 61430 M^{-1} cm^{-1}
Φ_f (rhodamine 6G in EtOH)= 0.02
IC_{50} (4T1 cells) = 0.325 μM (7.3 J cm^{-2})
IC_{50} (HS578t cells) = 0.285 μM (7.3 J cm^{-2})

PDT is widely reported to be able to enhance the antitumor immune responses, however elevated immune responses post-PDT depend on the effectiveness of the destruction of the tumor structure during PDT, which then effects infiltration of leukocytes and inflammatory mediators. Therefore, conjugating a ligand which can also elicit immune responses to the photosensitizer may further boost the overall antitumor immune responses. Notably, the IYIY-ligand itself was able to modulate immune responses in dark conditions, thereby playing an additional role other than receptor-based targeted delivery of the photosensitizer to cancer cells.[36] This opens the possibility of using ligand-conjugated BODIPY for immune- and photodynamic combination therapy.

Properties of peptide linkers used in conjugation, such as hydrophilicity and length, can affect the targeting efficiency. A study by Zhao *et al.* on targeting epidermal growth factor receptor (EGFR) used BODIPY (**23a**) conjugated to either a short-EGFR targeting pegylated peptide (to form **23b**) or a long-EGFR targeting pegylated peptide (to form **23c**). Both conjugates showed high cellular uptake compared to free BODIPY (**23a**) on EGFR-overexpressing Hep2 cells as observed in photocytotoxicity assay and fluorescence imaging study. The long peptidic **23c** had lower targeting ability compared to short peptidic **23b** due to its low aqueous solubility and high tendency to form aggregation, as there are 11 hydrophobic sites on the molecule (color in **23c**).[37] This was supported by surface plasmon resonance and docking study, where **23c** was shown to bind the lower side of the EGF binding pocket with the BODIPY core buried in the hydrophobic pocket. Conversely, **23b**

bound specifically to EGFR, away from the EGF binding pocket.

23a

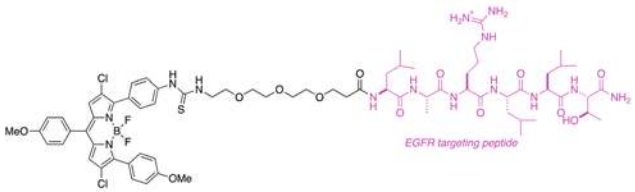

23b

DMSO
$\lambda_{max\ abs}$ = 588 nm
$\lambda_{max\ emiss}$ = 634 nm
log ε = 4.3 M^{-1} cm^{-1}
Φ_f (cresyl violet)= 0.033
Dark IC_{50} (Hep2 cells) = 98 μM (1.5 J cm^{-2})
Light IC_{50} (Hep2 cells) = 74 μM (1.5 J cm^{-2})

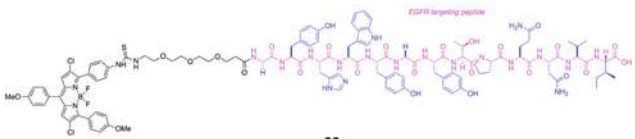

23c

DMSO
$\lambda_{max\ abs}$ = 586 nm
$\lambda_{max\ emiss}$ = 634 nm
log ε = 4.5 M^{-1} cm^{-1}
Φ_f (cresyl violet)= 0.014
Dark IC_{50} (Hep2 cells) = 180 μM (1.5 J cm^{-2})
Light IC_{50} (Hep2 cells) = > 100 μM (1.5 J cm^{-2})

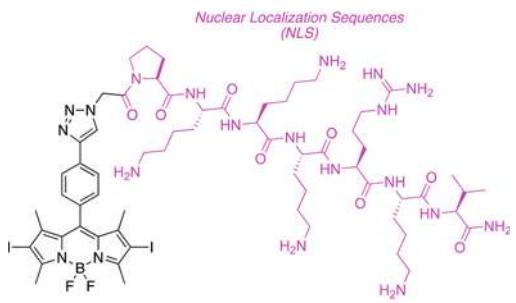

24

Methanol
$\lambda_{max\ abs}$ = 531 nm
$\lambda_{max\ emiss}$ = 549 nm
Φ_f (rhodamine 6G) = 2%
Dark IC_{50} (T24 cells) = > 10 μM (4 J cm^{-2})
Light IC_{50} (T24 cells) = 0.016 μM (4 J cm^{-2})

For ligand-targeted conjugates, the final subcellular destination of the conjugate may determine the photocytotoxicity efficiency of the conjugate. Direct targeting of the surface receptors will trigger receptor internalization, followed by localization in organelles. Organelle targeted conjugates can directly target the organelle of interest such as mitochondria to then activate the intrinsic pathway of apoptosis, or nuclei which contains DNA sensitive to oxidative damage by ROS. One such example was nuclear localization sequences (NLS)-I_2-BODIPY conjugate **24**, reported by Puckett *et al.* as a strategy to target the nucleus.[38] While NLS has been reported in the past to localize in the nucleus, the authors *did not* observe localization of **24** in nuclei but in lysosome and endoplasmic reticulum instead – a pattern that is similar to the unconjugated BODIPY.[39] Compared to the unconjugated BODIPY, **24** localized more in the ER with some minor liberation of the dye into the cytosol. This minor discrepancy in localization between **24** and the unconjugated BODIPY was translated to 2.6-fold greater photocytotoxicity in the urinary bladder carcinoma T24 cell line for **24**. Even though the author failed to target the nuclei, **24** showed improved photocytotoxicity as well as endosomal uptake, suggesting that a different targeting by the NLS ligand may have taken place.[40]

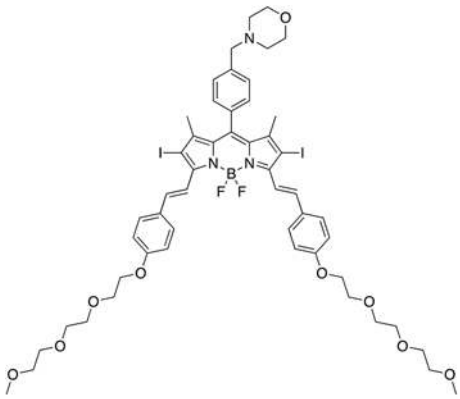

25

Acetonitrile/Toluene/MeOH/DCM
$\lambda_{max\ abs}$ = 660 nm
$\lambda_{max\ emiss}$ = 694 nm
ε = 83226 M^{-1} cm^{-1}
Φ_f = 0.11
$^1O_2$ QY = 0.64
Dark IC_{50} (MCF7) = N.D
Light IC_{50} (MCF-7 cells) = 0.2 μM (48 J cm^{-2})

Pegylated distyryl BODIPY (**25**) was designed to target the lysosomes. Upon uptake into MCF-7 cells, **25** was observed to localize in lysosomes and disrupted the lysosomal membrane depolarization upon irradiation, thereby releasing hydrolase to cytoplasm for onset of lysosome-mediated cell death. Compared to control photosensitizer chlorin e6, **25** showed seven-fold better photocytotoxicity (IC_{50} = 0.2 μM).[41]

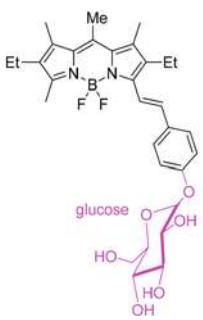

26

Ethanol
$\lambda_{max\ abs}$ = 573.8 nm
$\lambda_{max\ emiss}$ = 590 nm
ε = 82000 M^{-1} cm^{-1}
Φ_f (rhodamine) = 0.6
Dark IC_{50} (A549) = Non-determined up to 200 μM
Light IC_{50} (A549) = 2.7 ± 0.8 μM (0.77 mWcm^{-2})

Aiming for the high glucose uptake in cancer cells compared to normal cells, hydrophilic glycosylated BODIPY (**26**) was synthesized and studied.[42] Upon irradiation, complex **26** induced ROS-mediated apoptosis through the caspase-8/caspase-3 pathway on human lung A549 cancer cells (IC_{50} = 2.7 μM). When comparing its selectivity towards normal and cancer cells, complex **26** had 50% higher uptake and longer retention in A549 cells compared to normal L132 cells. The highest difference in cellular uptake between the normal and cancer cells was observed at 2 h, and this selectivity gradually disappeared and became comparable from 4 h onwards.

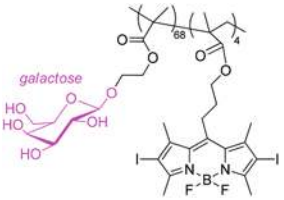

27a

PBS
$\lambda_{max\ abs}$ = 535 nm
$^1O_2$ QY (Rose Bengal) = 0.79
Cytotoxicity (HepG2 cells) = 3 – 20 %
(7.5 – 22.5 J cm^{-2})
Cytotoxicity (NIH3T3 cells) = 80 – 110 %
(7.5 – 22.5 J cm^{-2})

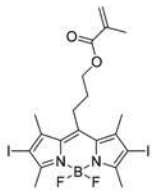

27b

CH_2Cl_2
$\lambda_{max\ abs}$ = 535 nm
$^1O_2$ QY (Rose Bengal) = 0.21
Cytotoxicity (HepG2 cells) = 20 – 40 %
(7.5 – 22.5 J cm^{-2})
Cytotoxicity (NIH3T3 cells) = 5 – 20 %
(7.5 – 22.5 J cm^{-2})

Li and co-workers reported a BODIPY-based macromolecular photosensitizer **27a**, which has tumor cell targeting galactose as a ligand for targeted PDT.[43] Galactose was chosen as it specifically binds to asialoglycoprotein (ASGP) receptors which are expressed only in the liver but not in other human tissues. Glycopolymer **27a** exhibited good water solubility even at 20 mg mL^{-1} in aqueous solution. **27a** was able to generate $^1O_2$ (Φ_Δ = 0.79) rapidly in aqueous systems but its hydrophobic diiodo-bodipy monomer (**27b**) could only generate $^1O_2$ (Φ_Δ = 0.21) when ethanol was used as the cosolvent. In confocal and flow cytometry studies, **27a** showed high cellular uptake on ASGP-overexpressing HepG2 liver cells compared to normal NIH3T3 cells, confirming targeting to the liver. This was further supported by the photocytotoxicity study, where **27a** showed enhanced selective killing of HepG2 cancer cells with 10% of cell viability compared to that of 80% cell viability of NIH3T3 cells under the same conditions (compound concentration of 20 μM, 10 min illumination). No dark cytotoxicity was observed.

II. Tunable BODIPY

Four pH- and thiol-dependent switchable BODIPYs (**28a–d**) were designed by Jiang *et al.*[44] The SOG and fluorescence activity in these BODIPY analogues were quenched by the proximate ferrocenyl moieties, which were attached *via* ketal- (**a**), disulphide- (**b**), ethylene (**c**) or a combination of ketal- and disulphide-linkers (**d**). The ketal linker was cleavable in the acidic environment whereas the disulphide linker was cleavable by dithiothreitol (DTT) or glutathione, which is 1000-fold more abundant in cancerous than normal cells.[45] The ethylene linker in **28c** was an uncleavable control. On MCF-7 cells and in the presence of DTT, **28d** was shown to have higher singlet oxygen generation and higher cellular uptake at pH 5.0 compared to pH 7.4. The analogues with only ketal (**28a**) or only disulphide linkers (**28b**) showed a high fluorescence intensity only at their respective cleavage environments, but not at combined acidic and high thiol environment. In their study on nude mice bearing HT29 human colorectal carcinoma, intratumoral injection of 2 μmol kg^{-1} of **28d** and non-cleavable **28c** revealed a high fluorescence intensity in the tumor region for **28d** but no fluorescence for the control (**28c**), suggesting that the acidic pH- and thiol-rich microenvironment of the tumor had activated the quenched BODIPY.

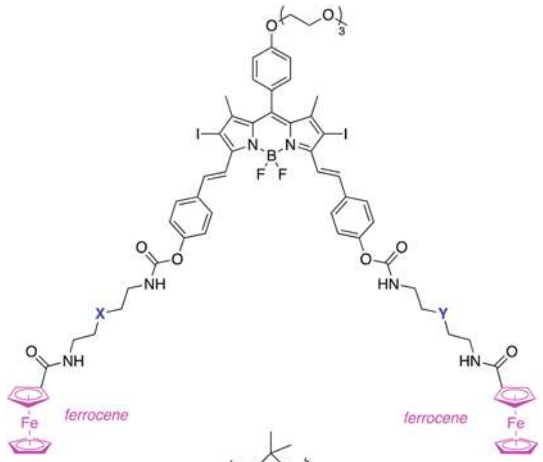

28a X = Y = ketal
28b X = Y = S–S
28c X = Y = CH_2CH_2
28d X = S–S Y = ketal

28d

PBS + 0.25% Cremophor EL
$\lambda_{max\ abs}$ = 376, 441, 662 nm
$\lambda_{max\ emiss}$ = 684-686 nm
Φ_f = 0.03-0.04
$^1O_2$ QY = 0.64
Dark IC_{50} (MCF-7 cells) = N.D
Light IC_{50} (MCF-7 cells)* = 140 nM (2 μM DTT), 81 nM (4 mM DTT)

* 48 J cm^{-2}

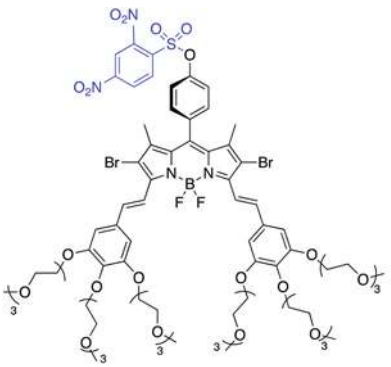

29

DMSO/PBS (1:1)
$\lambda_{max\ abs}$ = 660 nm
$\lambda_{max\ emiss}$ = 683 nm
Dark IC_{50} (HCT116 cells) = 4.38 μM
Light IC_{50} (HCT116 cells)* = 0.02 μM

* 660 nm, 4 h, 0.2 mW

A similar concept of a quenched BODIPY that only became activated to generate singlet oxygen after glutathione-mediated reaction was studied by Turan *et al.*[46] The quencher used was

2,4-dinitrobenzenesulfonate, which was linked to a brominated BODIPY (**29**) decorated with oligoethyleneglycol moieties for improved water solubility. As cancer cells express a high level of glutathione, a study to compare the efficacy in cancer and normal cell lines was carried out. An analogous unquenched derivative was also prepared and tested. The unquenched analogue had sub-micromolar IC_{50} (0.35–0.64 μM) in HCT116 human colon carcinoma cells. The quenched **29** showed high cellular uptake and, interestingly, even more potent photocytotoxicity than the unquenched analogue (IC_{50} ~ 0.02 μM) in HCT116 cells. **29** did not show photocytotoxic activity in normal human MRC-5 lung fibroblast cells, demonstrating its selectivity against cancer cells with high glutathione expression.

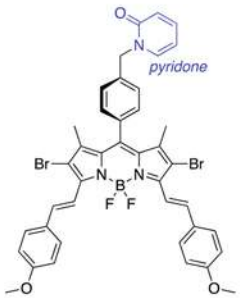

30a

DMSO
$\lambda_{max\ abs}$ = 668 nm
$\lambda_{max\ emiss}$ = 697 nm
ε = 22200 M^{-1} cm^{-1}
Φ_f = 0.14
$^1O_2$ QY (EtOH) = 0.15
CC_{50} (HeLa cells) = 49 nM

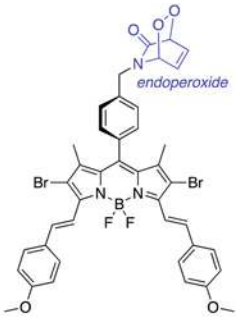

30b

DMSO
$\lambda_{max\ abs}$ = 667 nm
$\lambda_{max\ emiss}$ = 700 nm
ε = 74200 M^{-1} cm^{-1}
Φ_f = 0.10
$^1O_2$ QY (EtOH) = 0.20
CC_{50} (HeLa cells) = 8.6 nM

BODIPYs capable of cycloconversion can produce singlet oxygen species continuously both at irradiated (light) and non-irradiated (dark) conditions.[47] The 2,6-dibromo distyryl BODIPY/2-pyridone conjugate (**30a**) can generate singlet oxygen when irradiated at 650 nm, and a part of the singlet oxygen generated is trapped by **30a** to form 2-pyridone endoperoxide **30b**. In the absence of light, **30b** will undergo thermal cycloconversion to produce singlet oxygen and reform 2-pyridone conjugate **30a**. To compare the cytotoxic effect of **30a** and **30b**, HeLa cells were incubated with varying concentrations of **30a** and **30b** and illuminated for 10 minutes every hour, for 24 times (total irradiation time = 4 hours). Endoperoxide **30b** showed greater photocytotoxicity than 2-pyridone **30a** (the concentration of drug required to reduce cell viability by 50%, CC_{50} = 8.6 and 49.0 nM, respectively), probably because the endoperoxide state produced more singlet oxygen. This is important as oxygen molecules are generally exhausted after PDT, and cycloconvertible molecules such as **30b** will produce singlet oxygen in the dark without needing more oxygen from the microenvironment.

31a

Acetonitrile
$\lambda_{max\ abs}$ = 505 nm (+Zn^{2+}+phosphate)
$\lambda_{max\ emiss}$ = 518 nm (+Zn^{2+}+phosphate)
ε = 64200 M^{-1} cm^{-1} (+Zn^{2+}+phosphate)
Φ_f = 0.48 (+Zn^{2+}+phosphate)
$^1O_2$ QY (Eosin Y) = 0.10 (+Zn^{2+})
CC_{50} (K562 cells) = 365 nM

31b

Acetonitrile
$\lambda_{max\ abs}$ = 501 nm (+Zn^{2+}+phosphate)
$\lambda_{max\ emiss}$ = 517 nm (+Zn^{2+}+phosphate)
ε = 65800 M^{-1} cm^{-1} (+Zn^{2+}+phosphate)
Φ_f = 0.37 (+Zn^{2+}+phosphate)
$^1O_2$ QY (Eosin Y) = 0.11 (+Zn^{2+})

Akkaya and coworkers presented a molecular device based on a Zn^{2+}-terpyridine-bodipy conjugate **31**.[48] Conjugate **31b** was prepared for chemical characterization, while compound **31a** had additional solubilizing oligoethyleneglycol units suitable for experiments in biological media. The terpyridine unit binds Zn^{2+} ions strongly in aqueous solutions. In acetonitrile, **31b** had a very low fluorescence emission intensity and generated singlet oxygen efficiently in the presence of light, while the addition of phosphate ions resulted in a very sharp increase in emission intensity with concomitant loss of singlet oxygen generation. Similarly when exposed to light, the weakly-fluorescent **31a** initially generated singlet oxygen to trigger apoptosis in K562 cancer cells. Upon achieving apoptosis, **31a** then interacted with the exposed phosphotidylserines in the outer leaflet of the apoptotic cell membranes, autonomously switching off singlet oxygen generation and simultaneously switching on a bright emission response. This was evidenced in both flow cytometry and fluorescence microscopy experiments of the irradiated cells where co-staining with **31a** and PE-Annexin V was observed. The authors interpreted the workings of these conjugates as the response of a 1 : 2 molecular demultiplexer that takes light as an input and phosphatidylserines (**31a**) or phosphates ions (**31b**) as the switch; the two alternative outputs are singlet oxygen and fluorescence light.

III. Nanocarrier

The efficacy of BODIPY largely depends on the singlet oxygen generation efficiency upon light irradiation, selectivity towards tumor sites and minimal uptake by normal tissues. Various nanocarriers have been reported for their ability to enhance the efficacy of BODIPY by improving its water solubility, redu-

cing non-specific phototoxicity to non-tumor sites and increasing its antitumor efficacy by elevating its tumor accumulation *via* enhanced permeability and retention (EPR) effects. However, these nanocarriers are often limited by impaired singlet oxygen quantum yield within the nanocarriers, depletion of tissue oxygen in deeply-seated tumors and residual tumor cells which survived photodynamic cancer therapy.[49]

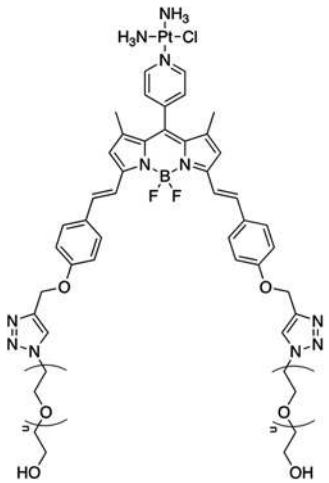

32

Aqueous
$\lambda_{max\ abs}$ = 680 nm
Φ_Δ = 0.34
Φ_T = 0.6
Light IC_{50} (4T1 cells) = 2.0×10^{-6} M

To maximize the antitumor efficacy of BODIPY, Guo *et al.* fabricated platinated BODIPY core (**32**) nanoparticles (Bodiplatin-NPs) for combined photodynamic cancer therapy and tumor thermal ablation.[50] The rationale for using platinum are two-fold: the high spin–orbit coupling constant (χ = 4481 cm^{-1}) of platinum atoms can promote rapid singlet-to-triplet ISC, and the unoccupied $d_{x^2-y^2}$ orbitals of square planar Pt(II) may provide easy nonradiative decay from excited state to ground state through the d–d energy band transition. Having these two properties, Bodiplatin-NPs can produce abundant reactive oxygen species (ROS) and potent hyperthermia at tumors under single-wave light irradiation. Bodiplatin-NPs showed effective intracellular translocation from lysosomes to cytoplasm, enhanced tumor accumulation, photoinduced cell damage and tumor ablation without any regrowth *via* the synergistic photodynamic and photothermal therapy.

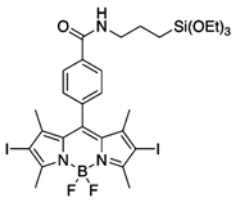

33

DMSO
$\lambda_{max\ abs}$ = 534 nm
$\lambda_{max\ emiss}$ = 560 nm
Φ_f = 1.3%

To enhance the ROS generation efficiency, Wang *et al.* incorporated BODIPY with two iodine atoms (**33**).[51] A silylated functional group was also added to covalently encapsulate the BODIPY into a silica matrix to form dye-doped nanoparticles, in order to reduce BODIPY leakage and the associated unwanted side effects. Approximately 58-fold quenching of the fluorescence compared to the control silylated BODIPY dye (without iodines) was demonstrated resulting from the heavy atom effect from the iodine. This was in agreement with the enhanced generation of singlet oxygen by the BODIPY-NPs as compared to the control dye-NPs. The BODIPY-NPs were successfully taken up by HeLa cells and showed photocytotoxicity against SKBR-3 cancer cells upon light irradiation. Moreover, the incorporated iodine atom can be replaced by a radiolabeled iodine atom (*e.g.*, I-124, I-125) to generate nanoparticles for position emission tomography (PET) imaging, demonstrating the potential development of a theranostic agent.

Wang *et al.* also incorporated two iodine atoms to the BODIPY core at 2- and 6-postions, but with an aryl carboxyl group at the *meso* position to link with the nanoscale UiO metal–organic frameworks (MOFs) (UiO-66) to form UiO-PDT nanocrystals. The UiO-66 MOFs consisted of inorganic {Zr6} clusters and benzenedicarboxylate (H2BDC) bridged linkers.[52] UiO-PDT nanocrystals showed higher cellular uptake in mouse melanoma cells B16F10 cells with increasing incubation time from 0.5 to 4 h. An increase of uptake rate of approximately 1.54-fold at 2 h was exhibited by the UiO-PDT nanocrystals as compared to that of free I_2-BDP. UiO-PDT nanocrystals demonstrated a lower ability to generate $^1O_2$ than I_2-BDP as a result of their heterogeneous nature. However, this did not impair their photocytotoxicty efficacy as 6.25 μg mL^{-1} concentration of the UiO-PDT sample showed a dramatic decline in cell viability to less than 20% for B16F10, CT26 and C26 cell lines. IC_{50} values for B16F10, CT26 and C26 are 0.70, 1.15 and 0.51 μg mL^{-1}, respectively.

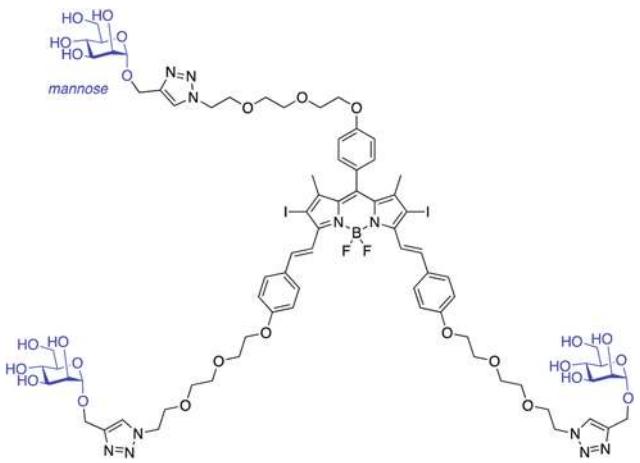

34

DMSO
$\lambda_{max\ abs}$ = 665 nm
$\lambda_{max\ emiss}$ = 678 nm
Φ_f = 0.17
$^1O_2$ QY = 0.58

Shallow light penetration depth had limited the application of BODIPYs to treat deeply-seated tumors, as currently available BODIPY dyes for PDT mostly require UV-vis light for activation. To obtain near infrared (NIR)-absorptive BODIPY dyes, Zhang

et al. incorporated distyryl moieties to I_2-BODIPY to shift the absorption to the long wavelength region with a maximum of 665 nm, to enable deep-tissue penetration.[53] In addition, mannose units were conjugated to the three-arm distyryl BODIPY (denoted as BTM or **34**) and co-assembled with Tween-80 to form BTM-loaded nanomicelles (denoted as BTM-NMs). The BTM-NMs exhibited much higher uptake by MDA-MB-231 cancer cells than by the MCF-10A non-cancer cells. Approximately a 2-fold increase in the red BTM fluorescence colocalized with the lysosomes was observed under confocal laser scanning microscopy in the absence of irradiation compared with the irradiated experimental conditions. This indicates that the BTM could escape from the lysosome after irradiation and re-distribute in the cytoplasm. MDA-MB-231 cells treated with the BTM-NMs demonstrated much lower cell viability than those treated with the BTG (glucose)-NMs, suggesting that the targeting effect of BTM-NMs through MR-mediated endocytosis increased the internalization of the NMs into MDA-MB-231 cells.

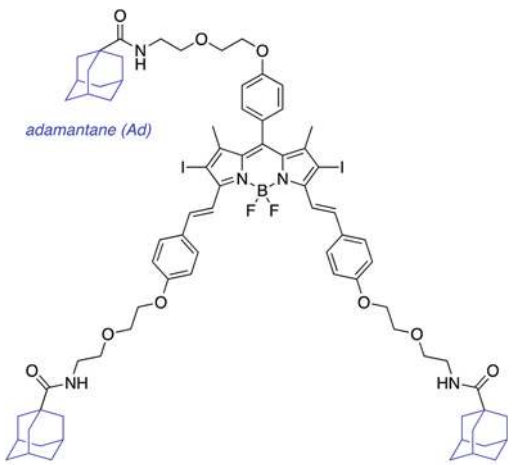

35

DMSO

$\lambda_{max\ abs}$ = 665 nm

Zhang *et al.*[54] also modified the three-arm distyryl BODIPY by conjugating with adamantane (Ad) units (denoted as BTA or **35**) in order to exhibit maximum absorption near 665 nm, again to allow for deep-tissue penetration. Heptamannosylated β-cyclodextrin (CD-Man7) was then immobilized onto the surface of BTA aggregates to function as a stabilizer for the formation of mannose-functionalized nanoparticles (BTA@CD-Man7). The mannose receptor (MR) is overexpressed on the surfaces of MDA-MB-231 breast cancer cells. BTA@CD-Man7 showed selective cellular uptake into MDA-MB-231 *via* MR-mediated endocytosis and was predominantly localized to lysosomes after 12 or 24 h of incubation. Conversely, the uptake of BTA@CD-Man7 into non-cancerous MCF-10A fibroblast cells was negligible. This facilitated $^1O_2$ generation specifically in cancer cells to induce apoptosis as demonstrated in the *in vitro* photocytotoxicity test in MDA-MB-231 cells. The targeted PDT efficacy of BTA@CD-Man7 was further evaluated using a mouse model that was established by injecting MDA-MB-231 cancer cells into subcutaneous tissues. BTA@CD-Man7 with irradiation inhibited the tumor to a significantly greater degree than BTA@CD and irradiation alone ($p < 0.01$). Hematoxylin and eosin (H&E) staining of tumor slices from mice treated with BTA@CDMan7 and irradiation exhibited severe tumor cell destruction in contrast to the tumor slices from control groups. Conversely, H&E staining of the heart, liver, kidney, lung, and spleen tissues of mice from different groups indicated no obvious abnormality or lesions. These results firmly demonstrated that BTA@CD-Man7 could be effectively used for *in vivo* targeted PDT with negligible adverse effects.

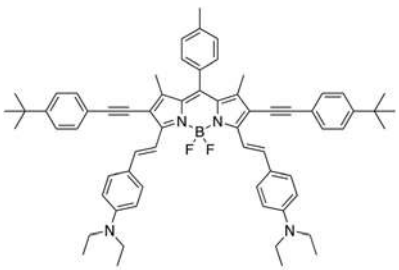

36

Dimethylformamide

$\lambda_{max\ abs}$ = 775 nm

$\varepsilon = 1.81 \times 10^4\ M^{-1}\ cm^{-1}$

Aqueous

$\lambda_{max\ abs}$ = 775 nm

Alternately, Hu *et al.* decorated the BODIPY core with a dimethylaminophenyl moiety to form bis-styryl BODIPY dye **36**.[55] The hydrophobic bis-styryl BODIPY dye was then encapsulated within amphiphilic DSPE-mPEG5000 to form water soluble BODIPY NPs. The BODIPY NPs demonstrated lysosome-targeting ability and enhanced photocytotoxicity in A549 cancer cells with their cell viability reduced by 2-fold as compared to that of indocyanine green. Tumor growth *in vivo* was significantly inhibited after the treatment of BODIPY NPs and laser without deteriorating the body weight of the tumor-bearing mice. Prominent necrosis and a higher level of cell apoptosis in the tumor tissue were also exhibited post-PDT.

Another common shortfall of nanocarriers is premature clearance by the reticuloendothelial system (RES). Voon *et al.*[56] reported the use of low molecular weight chitosan (25 kDa) coating on a poly(lactic-*co*-glycolic acid)-diiodinated boron dipyrromethene (PLGA-I_2BODIPY) nanoparticle-photosensitizer construct as "stealth coating" to reduce its serum protein adsorption and macrophage uptake. The PLGA-Chitosan-I_2BODIPY nanoparticles also exhibited better tumor-targeting selectivity and significantly reduced accumulation in RES tissues, including the lymph nodes, spleen and liver (by 10.2-, 2.1- and 1.3-fold, respectively compared to the PLGA nanoparticle without stealth coating), and in non-tumorous organs. These nanoparticles showed increased lysosomal cellular uptake, enhanced photocytotoxicity in 4T1 murine and

MDA-MB-231 human breast cancer cells *in vitro*, and increased anticancer efficacy in 4T1 tumor-bearing mice.

37

Chloroform
$\lambda_{max\ abs}$ = 721 nm
$\lambda_{max\ emiss}$ = 754 nm
ε = 89000 M^{-1} cm^{-1}
Φ_f = 0.45
$^1O_2$ QY (DBPF) = 0.36

Liu *et al.* designed an amphiphilic pH-responsive poly-oligo (ethylene glycol) methacrylate polymeric nanomaterial loaded with Br_2-BODIPY (**37**) at its hydrophobic pockets. The hydrophilic and hydrophobic segments undergo self-assembly at neutral pH to form a micelle and enlarged or disassembled its micelle at acidic pH to release BODIPY for PDT. Illumination (12 J cm^{-2}) at a concentration of 5.4 μM increased the mortality of the human liver HepG2 cells to 60%, which is 45% compared to the non-illuminated condition. For normal HL-7702 cells under the same treatment condition, there was 23% cell growth inhibition in the irradiated condition compared to that in the dark.[57]

IV. Multiple design strategy

Even as chemotherapy remains the main cancer treatment modality today, the side effects and lack of selectivity on cancer cells are still major concerns. Combination therapy, in this case PDT and chemotherapy, offers an opportunity for less harmful cancer treatment, as the drug dose of the respective treatments can ideally be reduced to eliminate undesirable side effects while achieving the same therapeutic outcome. However, co-treatment or co-administration of a cytotoxic drug and a photosensitizer does not always achieve the desired tumor selectivity, as the free cytotoxic drug may not accumulate sufficiently at the tumor site. To overcome this, various drug delivery systems have been designed to deliver multiple therapeutic agents (in this case, photosensitizer and cytotoxic drug) specifically to the tumor region, mainly through the enhanced permeability and retention effect or pH-mediated vesicle breakdown.[58]

Chemo-photodynamic therapy using supramolecular vesicles was studied. These vesicles consisted of building blocks of quaternary ammonium functionalized I_2-BODIPY (**38**, Fig. 1) linked to water soluble pillar[5]arene. The outer coat of the vesicles was the pillar[5]arene layer and doxorubicin (DOX) was loaded in the hydrophobic core (Fig. 1A).[59] At low pH, this vesicle disassembled to release cytotoxic DOX and BODIPY for PDT. DOX-loaded vesicles rapidly released approximately 80% of DOX at pH 5.1, compared to pH 6.0 (50%) and pH 7.4 (15%). Under irradiation conditions, the DOX loaded vesicles were cytotoxic to A549 cancer cells (IC_{50} = 1.4 μM), at 2-fold higher potency than the DOX free vesicles. In dark conditions, DOX-loaded vesicles had an IC_{50} of 5.5 μM, compared to DOX free vesicles, which had undetermined IC_{50} up to 20 μM.

Another example of pH-responsive DOX-encapsulated nanoparticles but with aza-BODIPY (**39**, Fig. 1) has been synthesized by Chen *et al.*[60] In this case, aza-BODIPY was selected for its capability to generate heat for photothermal therapy (PTT) and reactive oxygen species for photodynamic therapy (PDT). This approach applied the three-way combination of chemo-photodynamic-photothermal therapies. First, an acid-cleavable Schiff base between the amine group of DOX and the aldehyde group of polyethylene glycol (PEG) was prepared. The DOX-Aza-BODIPY (DAB) nanoparticles (Fig. 1B) were then formed by encapsulating aza-BODIPY with PEG-DOX. DAB was shown to release approximately 80% of DOX at pH 5.0, compared to 40% and 15% at pH 6.5 and 7.4, respectively. The released DOX was found to accumulate in the nucleus of cancer cells, which is the site of action of DOX chemotherapy. Under irradiation conditions in HeLa cells, DAB had an IC_{50} of 3.1 μg mL^{-1}, which was 2-fold lower than in the dark. In synergistic studies using 6 μg mL^{-1} DAB (equivalent to aza-BODIPY), PDT/PTT, chemo/PDT and chemo/PTT showed 47.7%, 41.3% and 32.8% of cell death, respectively, whereas chemo/PDT/PTT caused 71.6% of cell death. The synergistic effect was studied *in vivo* using the HeLa tumor model. Fifteen μg mL^{-1} (100 μL) of intravenous DAB with irradiation showed full elimination of tumor after 12 days with no tumor recurrence. Rapid accumulation of DAB in tumor was observed 1 h post injection and the level peaked at 6 h. In addition, the temperature of the tumor site increased to 46.7 °C within 10 minutes of irradiation compared to the PBS treated control group, which had a temperature of 38.8 °C.

A combination of receptor–ligand targeting (active targeting) and polymer micelle nanocarrier (passive targeting) for BODIPY can help to achieve higher selectivity against tumor cells. This was studied by the same researchers who prepared **37**,[61] this time using an amphiphilic polymer with the hydrophobic part (PLys) loaded with Br_2-BODIPY (**40**), and the hydrophilic part (POEGMA) for micelle stabilization. Galactose receptor targeted ligands (PMAGP) were then linked to the micelles to form a galactose functionalized copolymer (PMAGP-POEGMA-PLys-B, Fig. 1C). This targeted copolymer and a non-targeted vesicle were studied in galactose receptor expressing HepG2 cells and galactose receptor negative HeLa cells. The galactose targeted copolymer had higher photocytotoxicity in galactose expressing HepG2 cells (cell viability 50%) compared to non-galactose expressing HeLa cells (cell viability 72%). In fluorescence studies, the micelles mainly located in the cytoplasm and perinuclear region, and the fluorescence intensity of BODIPY increased over time, illustrating the endocytosis of the copolymers into cells. In addition, PMAGP-POEGMA-PLys-B demonstrated strong NIR fluorescence (721 nm) in HepG2 cells. These indicate the potential of BODIPY-loaded PMAGP-POEGMA-PLys-B micelles for theranosis of galactose expressing cancer types.

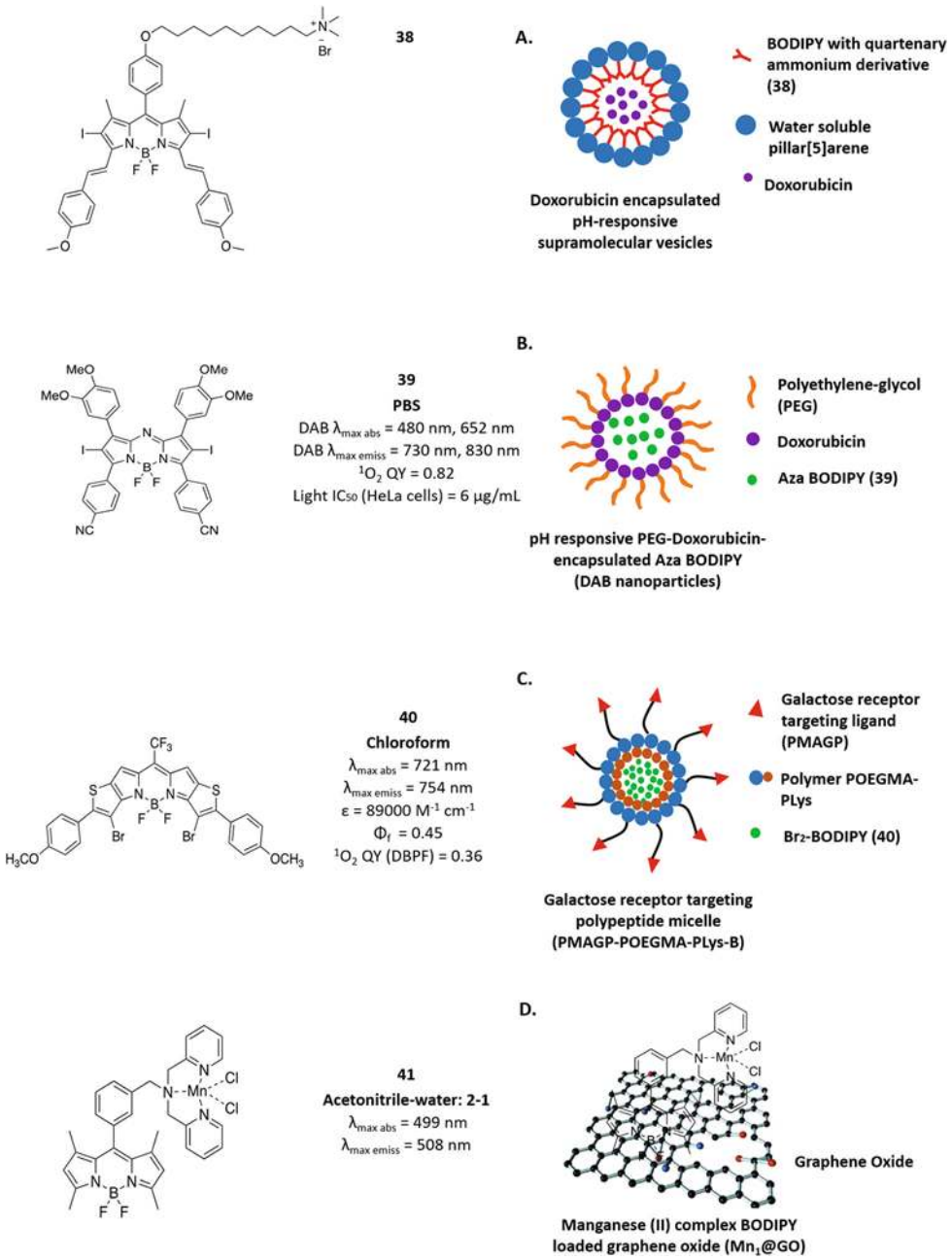

Fig. 1 Multiple design strategies of BODIPY derivatives with active and passive targeting agents for drug delivery.

A BODIPY based photoactive Mn(II) complex, denoted as Mn_1 (**41**, Fig. 1), loaded with graphene oxide (Mn_1@GO, Fig. 1D) was synthesized and studied.[62] Complex **41** was able to generate dioxygen when irradiated in water, while graphene oxide (GO) served as the drug delivery system. Cancer cells are more sensitive to H_2O_2 induced cell death than normal cells in hypoxic conditions; the Mn(II) complex was used to induce H_2O_2 production. Mn_1@GO and Mn_1 had comparable cytotoxicity (IC_{50} = 10 μM) on normal HepG2 cells. However in hypoxic conditions where the HepG2 cells were pre-treated with $CoCl_2$ for 24 h, active species Mn_1@GO@H_2O_2 (Mn_1@GO oxidized using H_2O_2) showed better inhibition (IC_{50} < 10 μM) than Mn_1 and Mn_1@GO (IC_{50} ~ 30 μM), suggesting additional anticancer activity from the dioxygen produced by the manganese species. Formation of Mn_1@GO@H_2O_2 and its anticancer activity could be accelerated in the presence of light. This approach capitalized on the sensitivity of cancer cells to H_2O_2 while BODIPY in this case functioned as a fluorescence probe.

Fig. 1 summarizes the BODIPY derivatives that were used for multiple design using active, passive or both drug delivery methods.

4. Conclusion

BODIPYs are valuable photosensitizers that possess extraordinary photophysical properties such as high intersystem crossing efficiency and singlet oxygen quantum yield, good photostability and low tissue toxicity. However, inherent limitations such as (i) inability to acquire energy from tissue penetrating near-infra-red (NIR) light for activation and (ii) tendency to aggregate in an aqueous environment have often hindered the advancement of BODIPY photosensitizers into clinical PDT. This review focuses on new approaches and strategies to develop better BODIPYs, to modulate and optimize their physicochemical properties in an attempt to address their weaknesses. The recent strategies introduced are highlighted and their merits and potential are discussed here. These include: (1) modification around the core structure of BODIPYs to enhance photophysical and photochemical properties, (2) conjugation with metal complexes to improve the photophysical properties, (3) conjugation with receptor ligands and other targeting molecules to increase the active accumulation of photosensitizers in tumors, (4) environment-response activatable BODIPYs in the tumor microenvironment, (5) association of BODIPYs to different nanocarriers to enhance water solubility and to actively or passively deliver photosensitizers to tumor, and (6) combination therapeutic strategies such as chemo-photodynamic-photothermal therapy to give synergistic effects.

It is noteworthy that the activities on some of the newly designed BODIPYs highlighted in this review have made serious headway into solving the classical limitations of BODIPY. BODIPYs **4**, **7**, **10d**, **32**, **36**, **37** and **40** (same structure as **37**) possess (i) enhanced structures for absorbing energy from deep-tissue-penetrating-NIR light (>680 nm) for photoactivation. Of these, BODIPYs **32**, **36**, **37** and **40** have further (ii) integrated the hydrophobic BODIPY into amphiphilic polymeric nanoparticles, so as to address the issue of aqueous instability which would have been worsened following (i). While some proof-of-concept studies in animals have been conducted for **36**, the others still need more data in this area. The next steps of development will need to include investigations into composition stability (which is a topic of much interest for nanoparticle-based drugs), formulation, pharmacokinetics, bioavailability and pharmacodynamic, and toxicology, as well as to review the clinical regulatory procedures for approval of nanoparticles in therapeutics.

Conflicts of interest

There are no conflicts to declare.

Acknowledgements

This research study was supported by Postgraduate Research Grant (PPP) – Research, project no. PG222-2016A.

References

1 A. Kamkaew, S. H. Lim, H. B. Lee, L. V. Kiew, L. Y. Chung and K. Burgess, *Chem. Soc. Rev.*, 2013, **42**, 77–88.
2 S. G. Awuah and Y. You, *RSC Adv.*, 2012, **2**, 11169–11183.
3 B. Kim, B. Sui, X. Yue, S. Tang, M. G. Tichy and K. D. Belfield, *Eur. J. Org. Chem.*, 2017, **2017**, 25–28.
4 J. Zou, Z. Yin, K. Ding, Q. Tang, J. Li, W. Si, J. Shao, Q. Zhang, W. Huang and X. Dong, *ACS Appl. Mater. Interfaces*, 2017, **9**, 32475–32481.
5 J. Wang, Y. Hou, W. Lei, Q. Zhou, C. Li, B. Zhang and X. Wang, *ChemPhysChem*, 2012, **13**, 2739–2747.
6 Y. Yang, Q. Guo, H. Chen, Z. Zhou, Z. Guo and Z. Shen, *ChemComm*, 2013, **49**, 3940–3942.
7 Y. Chen, J. Zhao, L. Xie, H. Guo and Q. Li, *RSC Adv.*, 2012, **2**, 3942–3953.
8 R. Lincoln, A. M. Durantini, L. E. Greene, S. R. Martinez, R. Knox, M. C. Becerra and G. Cosa, *Photochem. Photobiol. Sci.*, 2017, **16**, 178–184.
9 M. Pawlicki, H. A. Collins, R. G. Denning and H. L. Anderson, *Angew. Chem., Int. Ed.*, 2009, **48**, 3244–3266.
10 Y. Shen, A. J. Shuhendler, D. Ye, J.-J. Xu and H.-Y. Chen, *Chem. Soc. Rev.*, 2016, **45**, 6725–6741.
11 T. Zhang, R. Lan, L. Gong, B. Wu, Y. Wang, D. W. J. Kwong, W.-K. Wong, K.-L. Wong and D. Xing, *ChemBioChem*, 2015, **16**, 2357–2364.
12 R. L. Watley, S. G. Awuah, M. Bio, R. Cantu, H. B. Gobeze, V. N. Nesterov, S. K. Das, F. D'Souza and Y. You, *Chem. – Asian J.*, 2015, **10**, 1335–1343.
13 X. F. Zhang and N. Feng, *Chem.– Asian J.*, 2017, **12**, 2447–2456.
14 Y.-C. Lai, S.-Y. Su and C.-C. Chang, *ACS Appl. Mater. Interfaces*, 2013, **5**, 12935–12943.
15 N. Epelde-Elezcano, E. Palao, H. Manzano, A. Prieto-Castaneda, A. R. Agarrabeitia, A. Tabero, A. Villanueva, S. de la Moya, I. Lopez-Arbeloa, V. Martinez-Martinez and M. J. Ortiz, *Chemistry*, 2017, **23**, 4837–4848.
16 X. Cui, J. Zhao, Z. Mohmood and C. Zhang, *Chem. Rec.*, 2016, **16**, 173–188.
17 Y. You and W. Nam, *Chem. Soc. Rev.*, 2012, **41**, 7061–7084.
18 P. Majumdar, X. Yuan, S. Li, B. Le Guennic, J. Ma, C. Zhang, D. Jacquemind and J. Zhao, *J. Mater. Chem. B*, 2014, **2**, 2838–2854.
19 E. Palao, R. Sola-Llano, A. Tabero, H. Manzano, A. R. Agarrabeitia, A. Villanueva, I. Lopez-Arbeloa, V. Martinez-Martinez and M. J. Ortiz, *Chemistry*, 2017, **23**, 10139–10147.
20 L. Tabrizi and H. Chiniforoshan, *RSC Adv.*, 2017, **7**, 34160–34169.
21 Y. Liu, N. Song, L. Chen and Z. G. Xie, *Chin. J. Polym. Sci.*, 2018, **36**, 417–424.
22 K. D. Mjos and C. Orvig, *Chem. Rev.*, 2014, **114**, 4540–4563.
23 C. Mari, V. Pierroz, S. Ferrari and G. Gasser, *Chem. Sci.*, 2015, **6**, 2660–2686.
24 T. Wang, Y. Hou, Y. Chen, K. Li, X. Cheng, Q. Zhou and X. Wang, *Dalton Trans.*, 2015, **44**, 12726–12734.

25 J. Chalissery, D. Jalal, Z. Al-Natour and A. H. Hassan, *DNA Repair*, 2017, **51**, 2–13.
26 A. Bhattacharyya, A. Dixit, K. Mitra, S. Banerjee, A. A. Karande and A. R. Chakravarty, *Med. Chem. Commun.*, 2015, **6**, 846–851.
27 N. Mukherjee, S. Podder, K. Mitra, S. Majumdar, D. Nandi and A. R. Chakravarty, *Dalton Trans.*, 2018, **47**, 823–835.
28 U. Bhattacharyya, B. Kumar, A. Garai, A. Bhattacharyya, A. Kumar, S. Banerjee, P. Kondaiah and A. R. Chakravarty, *Inorg. Chem.*, 2017, **56**, 12457–12468.
29 K. Mitra, S. Gautam, P. Kondaiah and A. R. Chakravarty, *ChemMedChem*, 2016, **11**, 1956–1967.
30 M. K. Raza, S. Gautam, A. Garai, K. Mitra, P. Kondaiah and A. R. Chakravarty, *Inorg. Chem.*, 2017, **56**, 11019–11029.
31 Y. Liu, Z. Li, L. Chen and Z. Xie, *Dyes Pigm.*, 2017, **141**, 5–12.
32 M. Ucuncu, E. Karakus, E. Kurulgan Demirci, M. Sayar, S. Dartar and M. Emrullahoglu, *Org. Lett.*, 2017, **19**, 2522–2525.
33 C. S. Kue, A. Kamkaew, K. Burgess, L. V. Kiew, L. Y. Chung and H. B. Lee, *Med. Res. Rev.*, 2016, **36**, 494–575.
34 A. Kamkaew and K. Burgess, *J. Med. Chem.*, 2013, **56**, 7608–7614.
35 C. S. Kue, A. Kamkaew, H. B. Lee, L. Y. Chung, L. V. Kiew and K. Burgess, *Mol. Pharm.*, 2015, **12**, 212–222.
36 C. S. Kue, A. Kamkaew, S. H. Voon, L. V. Kiew, L. Y. Chung, K. Burgess and H. B. Lee, *Sci. Rep.*, 2016, **6**, 37209.
37 N. Zhao, T. M. Williams, Z. Zhou, F. R. Fronczek, M. Sibrian-Vazquez, S. D. Jois and M. G. H. Vicente, *Bioconjugate Chem.*, 2017, **28**, 1566–1579.
38 C. A. Puckett and J. K. Barton, *Bioorg. Med. Chem.*, 2010, **18**, 3564–3569.
39 P. Verwilst, C. C. David, V. Leen, J. Hofkens, P. A. de Witte and W. M. De Borggraeve, *Bioorg. Med. Chem. Lett.*, 2013, **23**, 3204–3207.
40 J. Gruenberg and H. Stenmark, *Nat. Rev. Mol. Cell Biol.*, 2004, **5**, 317–323.
41 M. Li, R. Tian, J. Fan, J. Du, S. Long and X. Peng, *Dyes Pigm.*, 2017, **147**, 99–105.
42 N. Shivran, M. Tyagi, S. Mula, P. Gupta, B. Saha, B. S. Patro and S. Chattopadhyay, *Eur. J. Med. Chem.*, 2016, **122**, 352–365.
43 Z. Lu, X. Zhang, Z. Wu, T. Zhai, Y. Xue, L. Mei and C. Li, *RSC Adv.*, 2014, **4**, 19495–19501.
44 X. J. Jiang, J. T. Lau, Q. Wang, D. K. Ng and P. C. Lo, *Chemistry*, 2016, **22**, 8273–8281.
45 M. P. Gamcsik, M. S. Kasibhatla, S. D. Teeter and O. M. Colvin, *Biomarkers*, 2012, **17**, 671–691.
46 I. S. Turan, F. P. Cakmak, D. C. Yildirim, R. Cetin-Atalay and E. U. Akkaya, *Chemistry*, 2014, **20**, 16088–16092.
47 I. S. Turan, D. Yildiz, A. Turksoy, G. Gunaydin and E. U. Akkaya, *Angew. Chem., Int. Ed.*, 2016, **55**, 2875–2878.
48 I. S. Turan, G. Gunaydin, S. Ayan and E. U. Akkaya, *Nat. Commun.*, 2018, **9**, 805.
49 S. H. Voon, L. V. Kiew, H. B. Lee, S. H. Lim, M. I. Noordin, A. Kamkaew, K. Burgess and L. Y. Chung, *Small*, 2014, **10**, 4993–5013.
50 Z. Guo, Y. Zou, H. He, J. Rao, S. Ji, X. Cui, H. Ke, Y. Deng, H. Yang, C. Chen, Y. Zhao and H. Chen, *Adv. Mater.*, 2016, **28**, 10155–10164.
51 Z. Wang, X. Hong, S. Zong, C. Tang, Y. Cui and Q. Zheng, *Sci. Rep.*, 2015, **5**, 12602.
52 W. Wang, L. Wang, Z. Li and Z. Xie, *ChemComm*, 2016, **52**, 5402–5405.
53 Q. Zhang, Y. Cai, Q. Y. Li, L. N. Hao, Z. Ma, X. J. Wang and J. Yin, *Chemistry*, 2017, **23**, 14307–14315.
54 Q. Zhang, Y. Cai, X.-J. Wang, J.-L. Xu, Z. Ye, S. Wang, P. H. Seeberger and J. Yin, *ACS Appl. Mater. Interfaces*, 2016, **8**, 33405–33411.
55 W. Hu, H. Ma, B. Hou, H. Zhao, Y. Ji, R. Jiang, X. Hu, X. Lu, L. Zhang, Y. Tang, Q. Fan and W. Huang, *ACS Appl. Mater. Interfaces*, 2016, **8**, 12039–12047.
56 S. H. Voon, S. X. Tiew, C. S. Kue, H. B. Lee, L. V. Kiew, M. Misran, A. Kamkaew, K. Burgess and L. Y. Chung, *J. Biomed. Nanotechnol.*, 2016, **12**, 1431–1452.
57 L. Liu, L. Fu, T. Jing, Z. Ruan and L. Yan, *ACS Appl. Mater. Interfaces*, 2016, **8**, 8980–8990.
58 Y. Lv, L. Hao, W. Hu, Y. Ran, Y. Bai and L. Zhang, *Sci. Rep.*, 2016, **6**, 29321.
59 L. B. Meng, W. Zhang, D. Li, Y. Li, X. Y. Hu, L. Wang and G. Li, *ChemComm*, 2015, **51**, 14381–14384.
60 D. Chen, Q. Tang, J. Zou, X. Yang, W. Huang, Q. Zhang, J. Shao and X. Dong, *Adv. Healthcare Mater.*, 2018, e1701272.
61 L. Liu, Z. Ruan, T. Li, P. Yuan and L. Yan, *Biomater. Sci.*, 2016, **4**, 1638–1645.
62 X.-L. Xu, J. Shao, Q.-Y. Chen, C.-H. Li, M.-Y. Kong, F. Fang, L. Ji, D. Boison, T. Huang, J. Gao and C.-J. Feng, *J. Inorg. Biochem.*, 2016, **159**, 1–6.

